Thesis

ADVANCING IONTRONIC IMPLANTS: TARGETED CHEMOTHERAPY WITH GEMCITABINE FOR GLIOBLASTOMA MULTIFORME

submitted by

Marilena Knittelfelder

in partial fulfillment of the requirements for the degree of

Doktorin der gesamten Heilkunde

(Dr^{in}. med. univ.)

at the

Medical University of Graz

executed at the

Gottfried Schatz Forschungszentrum

under the supervision of

Assoz. Prof. Priv.-Doz. Dipl.-Ing. Dr.techn. Rainer Schindl

Linda Waldherr, M.Sc., Ph.D.

Graz, 15.09.2023

Declaration of Academic Integrity

I hereby confirm that the present diploma thesis is the result of my own independent scholarly work. I also confirm that in all cases, where material from the work of others (in books, articles, essays, dissertations, and on the internet) is acknowledged, quotations and paraphrases are clearly indicated. No material other than that cited in the reference list has been used. I have read and understood the Medical University's regulations and procedures concerning plagiarism.

Graz, 15.09.2023 *Marilena Knittelfelder m.p.*

Acknowledgments

As I complete this thesis and my degree to become a medical professional, I am filled with profound gratitude and humbled by the journey which has been nothing short of transformative.

First and foremost, my sincere appreciation goes to my supervisors Linda Waldherr, M.Sc., Ph.D. and Assoc. Prof. Priv.-Doz. Dipl.-Ing. Dr.techn. Rainer Schindl. As they introduced me to the world of biomedical research, their guidance and assistance proved to be invaluable.

I would also like to extend my heartfelt gratitude to Univ.-Ass. Priv.-Doz. Mag. Dr.rer.nat. Nassim Ghaffari Tabrizi-Wizsy, Manuela Pirker, M.Sc., Peter Possert, Verena Handl, M.Sc., Sabine Erschen, and Georg Tsangarakis, whose active support made it possible to complete this thesis.

Behind every successful individual, there exists an unyielding pillar of strength, and in my case, this pillar comprises my family, my cherished loved ones, and my steadfast friends. Your unwavering support has been the beacon guiding me through the darkest storms and the source of all joy in my triumphs.

I would also like to pay tribute to my beloved parents, Karla and Werner. Your unconditional love and enduring support have fortified me through every step of my journey – you are my guiding lights and the cornerstones of all my achievements.

To my best friend, Dr. med.univ. Polina Mantaj, our friendship has been an unbreakable bond for a decade and an anchor in the tumultuous sea of academia. Through shared laughter, hardships, and triumphs, we evolved as individuals and embraced our roles as doctors.

And lastly, I would like to extend my heartfelt thanks to Dominik: you have been my rock, my unwavering support, and my joy. Your love has been the inspiration to push the boundaries of my capabilities, and your presence has illuminated even the darkest days.

Thank you.

Zusammenfassung

Hintergrund: Das Glioblastoma multiforme (GBM) ist der häufigste maligne Hirntumor im Erwachsenenalter. Trotz chirurgischer Tumorresektion, intensiver systemischer Chemotherapie mit Temozolomid (TMZ) und konkomitanter Strahlentherapie beträgt die mittlere Überlebensrate 15 Monate nach Diagnosestellung. Besonders problematisch gestaltet sich die begrenzte Auswahl an chemotherapeutischen Medikamenten aufgrund ihrer Unfähigkeit, die Blut-Hirn-Schranke zu überwinden.

Die Entwicklung der organisch elektronischen Ionenpumpe (OEIP) zur lokalen Chemotherapie beim GBM könnte den Einsatz neuer und wirksamerer chemotherapeutische Wirkstoffe, wie z.B. Gemcitabin (Gem) ermöglichen. In dieser Studie wurde der antineoplastische Effekt des Chemotherapeutikums Gem im Vergleich zum derzeitigen Goldstandard TMZ in drei verschiedenen GBM-Zellreihen untersucht.

Methodik:

Im *in vitro* Abschnitt der Studie wurden die jeweiligen IC_{50}-Werte von Gem und TMZ an den GBM-Zelllinien A-172, U-251 MG und LN-18 ermittelt. In diesem Zusammenhang wurden die Zellen über einen Zeitraum von 72 Stunden hinweg mit steigenden Medikamentendosierungen behandelt. Aus den jeweilig erhobenen Daten wurde der Mittelwert bestimmt und mittels der Prism GraphPad Software die IC_{50}-Werte statistisch ausgewertet.

Um die Ergebnisse in einer *in vivo* Umgebung zu überprüfen, wurden GBM-Tumore der Zelllinie LN-18 auf der chorioallantoischen Membran (CAM) von Hühnerembryonen kultiviert und mit einer singulären Verabreichung von 100 µM Gem oder 1.5 mM TMZ behandelt. Die behandelten Tumore wurden mit einer unbehandelten Kontrollgruppe verglichen. Nach immunhistochemischer Färbung wurden Ki-67 positive Tumorzellen mittels der histoanalytischen Software QuPath ermittelt und der Ki-67 Proliferationsindex zur Auswertung errechnet.

Ergebnisse: Im Rahmen der *in vitro* Experimente konnte eine bis zu 10^5-fache potentere antineoplastische Wirkung von Gem im Vergleich zu TMZ festgestellt werden. Jedoch zeigte sich unter *in vivo* Konditionen kein signifikanter Unterschied zwischen den drei Behandlungsgruppen ($p=0.417$).

Conclusio: Die ermittelten IC_{50}-Werte von Gem und TMZ zeigten im Vergleich, dass Gem bereits bei deutlich niedrigeren Konzentrationen eine antineoplastische Wirkung auf die GBM-Zellen A-172, U-251 MG und LN-18 hat. Auch wenn das in vivo Modell keine Signifikanz zwischen den drei Behandlungsgruppen zeigte, ist dies durch das Behandlungsschemata mit einer singulären Behandlung zu erklären.

Abstract

Background: Glioblastoma multiforme (GBM) is the most common malignant brain tumor in adults. Despite surgical resection, intensive systemic chemotherapy with Temozolomide (TMZ), and concurrent radiotherapy, the average survival period after diagnosis is only 15 months. The limited selection of chemotherapeutic drugs available for GBM treatment is particularly challenging, as most drugs are unable to penetrate the blood-brain barrier (BBB).

The development of the organic electronic ionic pump (OEIP) for local chemotherapy in GBM could enable the use of novel and more effective chemotherapeutic agents, such as Gemcitabine (Gem). This study examined the antineoplastic effect of the chemotherapeutic agent Gem compared to the current gold standard, TMZ, in three different GBM cell lines.

Methods: In the *in vitro* part of the study, the respective IC_{50} values of Gem and TMZ were determined in the GBM cell lines A-172, U-251 MG, and LN-18. The cells were treated with a wide range of drug concentrations for 72 hours (h). The mean value was calculated from the collected data and statistically analyzed using Prism GraphPad software. To verify the results in an *in vivo* environment, GBM tumors of the LN-18 cell line were cultivated on the chorioallantoic membrane (CAM) of chicken embryos and treated with a singular administration of 100 µM Gem or 1.5 mM TMZ. The treated tumors were compared with an untreated control group. After immunohistochemical staining, Ki-67-positive tumor cells were determined using the histoanalytical software QuPath, and the Ki-67 proliferation index was calculated for evaluation.

Results: An up to 10^5-fold more potent antineoplastic effect of Gem compared to TMZ was observed in the *in vitro* experiments. However, under *in vivo* conditions, no significant difference between the three treatment groups ($p = 0.417$) was found.

Conclusion: The IC_{50} values of Gem and TMZ that were determined demonstrated that Gem has an antineoplastic effect on all three GBM cell lines at significantly lower concentrations. While the results of the *in vivo* model did not show any significance between all three treatment groups, this outcome can be attributed to the treatment regimen of one singular drug administration.

Inhaltsverzeichnis

Acknowledgments ..... **I**

Zusammenfassung ..... **II**

Abstract ..... **IV**

Abbreviations ..... **VII**

List of figures ..... **IX**

List of tables ..... **XI**

1 Introduction **1**

1.1 Glioblastoma multiforme **1**

1.1.1 Definition 1

1.1.2 Classification 1

1.1.3 Epidemiology 2

1.1.4 Pathogenesis 4

1.1.5 MGMT promoter status 5

1.1.6 Pathology 6

1.1.7 Outcome and prognosis 7

1.1.8 Clinical presentation 8

1.1.9 Current treatment approaches 8

1.2 Organic electronic ionic pumps **10**

1.3 Temozolomide **12**

1.3.1 Resistance of glioblastoma cells against temozolomide 12

1.4 Gemcitabine **13**

1.5 Chicken chorioallantoic membrane assay **14**

2 Aims of this study **15**

3 Materials und Methods **16**

3.1 Cell lines **16**

3.2 Cell culture **17**

3.3 IC_{50} determination **18**

3.3.1 Experimental setup for IC_{50} determination 18
3.3.2 MTS assay 19
3.3.3 Statistical analysis of the IC_{50} values 19
3.4 Preparation for the CAM assay 20
3.4.1 LN-18 cultivation on CAM 21
3.4.2 Preparation of LN-18 cells for xenografting 23
3.4.3 Xenografting 23
3.4.4 Treatment of LN-18 onplants 24
3.4.5 Harvest, fixation, and paraffin-embedding of onplants 24
3.5 Histological analysis 26
3.5.1 Hematoxylin eosin staining 26
3.6 Immunohistochemistry – Ki-67-staining 27
3.6.1 Ki-67 proliferation index 27
3.6.2 Quantification of positive cells with QuPath 27
3.6.3 Statistical analysis of Ki-67 indexes 28
4 Results 30
4.1 IC_{50} curves of TMZ 30
4.2 IC_{50} curves of Gem 32
4.3 CAM assay results 36
4.3.1 HE staining 36
4.3.2 Ki-67 proliferation index 44
4.3.3 Immunohistochemical quantification – statistical evaluation of the Ki-67 proliferation index 45
5 Discussion 48
References 51

Abbreviations

AEM	anion exchange membrane
BBB	blood brain barrier
bc	blank corrected
CAM	chicken chorioallantoic membrane
CBTRUS	Central Brain Tumor Registry of the United States
CEM	cation exchange membrane
CNS	central nervous system
df	degrees of freedom
dFdU	2',2'-difluorodeoxyuridine
D-MEM	Dulbecco's Modified Eagle's Medium
DMSO	Dimethyl sulfoxide
DNA	deoxyribonucleic acid
EGF	epidermal growth factor
EGFR	epidermal growth factor receptor
FBS	fetal bovine serum
GC	growth control
GBM	Glioblastoma Multiforme
Gem	Gemcitabine
GSCs	glioma stem cells
h	hours
H	H-value
H3	histone 3
HE	hematoxylin-eosin
ICP	intracranial pressure
IDH	isocitrate dehydrogenase

IR	incidence rate
MGMT	O^6-methylguanine-DNA-methyltransferase
MIB-1	Molecular Immunology Borstel
min	minutes
MTIC	5- (3-methyltriazen-1-yl) imidazole-4-carboxamide
MTS	CellTiter 96® AQ_{ueous} Non-Radioactive Cell Proliferation
N	number
OEIP	organic electronic ionic pump
P	p-value
PBS	phosphate buffer saline
PCR	polymerase chain reaction
PDFG	platelet-derived growth factor
PFA	paraformaldehyde
PI3K	phosphatidylinositol-3-OH-kinase
PTEN	phosphatase and tensin homolog
RB	retinoblastoma
RNA	ribonucleic acid
RT	room temperature
RTK	receptor tyrosine kinase
SD	Standard Deviation
TMZ	Temozolomide
TTF	tumor treating fields
UV	ultraviolet
VEGF	vascular endothelial growth factor
WHO	World Health Organization

List of figures

Figure 1. Age and gender-specific IR for GBM, adjusted for age according to the data from the CBTRUS statistical report; reproduced with the permission of the publisher “American Association for Cancer Research”according to license number 1218339-1 (RightsLink®). 3

Figure 2. Schematic representation of an OEIP filled with drug. As an electric current is applied, the drug molecules travel through the channel via electrophoresis to their target site. 11

Figure 3. Chicken embryo ex ovo (day 10 of development) (property of Manuela Pirker, M.Sc., and used with permission)..... 21

Figure 4. Macroscopic image of the harvested xenograft in a sterile Petri dish containing PBS. 25

Figure 5. Screenshot of the parameters used for positive cell detection in QuPath. 28

Figure 6. TMZ IC_{50} curves of GBM cell lines A-172 (green), U-251 MG (blue), and LN-18 (red) after 72 h of treatment with increasing TMZ concentrations. All data points are shown as a mean from n = 3 ± SD in LN-18 and U-251 MG and n = 6 ± SD in A-172. 32

Figure 7. Comparison of all Gem-IC_{50} curves of GBM cell lines A-172 (green), U-251 MG (blue), and LN-18 (red) after 72 h of treatment. All data points for A-172 and U-251 are shown as a mean of n = 6 from two experimental runs, while all data points for LN-18 are shown as a mean of n = 3 ± SD from one experimental run. 34

Figure 8. IC_{50} curves of Gem and TMZ in all three GBM cell lines in comparison, data re-used from figure 6 and figure 7. All cells were treated for 72 hours, and cell viability was assessed using the MTS assay. The labeling of SD was omitted to ensure better clarity and overview. 35

Figure 9. Untreated tumor of the cell line LN-18 on CAM as a representative of the xenografts (4x magnification). The arrows highlight the key components CAM (green arrows), blood vessels (red arrows), and the tumor itself (black arrow). 36

Figure 10. Images 1-4 are representative results of the HE-stained LN-18 xenografts from all three treatment conditions. Images 5a-c show each tumor in their respective Ki-67 staining. Each tumor is photographed in 4x, 10x, 20x and 40x magnification and their respective Ki-67 stain. Images 1-5a shows a xenograft of the GC group, Images 1-5b shows

a tumor treated with Gem 100 µM and Images 1-5c shows the tumor treated with 1.5 mM TMZ. Images 3a-c show the invasion of tumor cells into the CAM. 38

Figure 11. HE-stained LN-18 tumors on CAM treated with a single topical treatment of 20 µL solution with a TMZ concentration of 1.5 mM, followed by 72 h of incubation, displayed in 4x magnification. 39

Figure 12. HE-stained slides with tumors of GBM cell line LN-18 on CAM after one single topical treatment with 20 µL of Gem in 100 µM concentration, followed by 72 h of incubation (4x magnification). Gem-treated tumors were prone to breakage while slicing and the superficial tumor on the CAM showed breakage and less density compared to those in the GC group. An invasion of the GBM cells in the CAM was observed..... 40

Figure 13. LN-18 tumors on CAM in the GC group received no treatment with any drug and were incubated for 72 h alongside the two treatment groups (HE-staining, 4x magnification). The untreated xenografts have a dense tissue composition and show a pronounced tumor cell invasion into the CAM. 41

Figure 14. Microscopic comparison of an HE-stained slide of one xenograft of the untreated GC group in Image a (4x magnification) and one xenograft in the Gem group in Image b (10x magnification). Gem-treated tumors were more prone to breakage on the surface as shown in Figures 14c and 15. All three treatment groups showed tumor invasion into the CAM (red arrows). 42

Figure 15. HE-slides of Gem-treated LN-18 tumors on CAM with low tumor cell cohesion in x10 magnification. The Gem-treated tumors exhibited a higher susceptibility to breakage, both during tumor harvesting and the subsequent slicing process for preparing microscopic slides. 43

Figure 16. Ki-67 stained GBM tumor of cell line LN-18 on CAM for reference (10x magnification). In the zoomed area (16.4x magnification) Ki-67 positive cells are brown (red arrows) while Ki-67 negative cells are blue (yellow arrows). 44

Figure 17. Box plot of the Ki-67 indexes of all treatment groups with the SD and distribution of individual Ki-67 index values within each treatment group. 46

List of tables

Table 1. Properties and information concerning the GBM cell lines employed 16

Table 2. Growth rate, splitting ratio and splitting frequency in the three GBM cell lines. . 17

Table 3. Setup of CAM assay #169 with LN-18 and three treatment conditions..... 21

Table 4. Setup of CAM assay #174 with LN18 and three treatment conditions..... 22

Table 5. Setup of CAM assay #175 with LN-18 and three treatment conditions..... 22

Table 6. Volume and composition of the cell suspension per onplant. The cell suspension with medium supplied nutrients to the system while the carrier matrix counteracted cell dispersion. 23

Table 7. The embedding protocol followed for the paraffinization of the harvested xenografts 25

Table 8. HE staining protocol..... 26

Table 9. Mean cell viability (%) and SD in GBM cell line LN-18 after 72 h of treatment with different TMZ concentrations. N = 3 for each concentration in one experimental run..... 30

Table 10. Mean cell viability (%) and SD in GBM cell line A-172 after 72 h of treatment with varying TMZ concentrations. N = 6 from two independent experiments. 31

Table 11. Mean cell viability (%) and SD in GBM cell line U-251 MG after 72 h of treatment with varying TMZ concentrations (µM). N = 3 in one experimental run. 31

Table 12. IC_{50} values of TMZ in GBM cell lines A-172, U-251 MG, and LN-18 after 72 h of treatment. 31

Table 13. Mean cell viability (%) and SD in GBM cell line LN-18 after 72 h treatment with increasing Gem concentration and n = 3 from one experimental run. 33

Table 14. Mean cell viability (%) in GBM cell line A-172 after 72 h of treatment with different Gem concentrations. The data is shown as mean of n = 6 ± SD from two independent experimental runs. 33

Table 15. Mean cell viability (%) and SD of GBM cell line U-251 MG after 72 h of treatment with different Gem concentrations. The mean cell viability was determined from n = 6 ± SD from two independent experimental runs. 34

Table 16. IC_{50} values of Gem in GBM cell lines A-172, U-251 MG, and LN-18 35

Table 17. The Shapiro-Wilk test of gathered data does not indicate a normal distribution. 45

Table 18. The Shapiro-Wilk test showed normal distribution after outlier correction..... 45

Table 19. The median and mean Ki-67 indexes (%) of LN-18 tumors that were determined for three treatment conditions: Gem 100 µM, TMZ 1.5 mM, and a GC group with no treatment. The results were obtained by using the QuPath software to accurately identify the Ki-67 positive cells following immunohistochemical staining. 46

Table 20. The results derived from the Kruskal-Wallis test to determine the p of the CAM assays of the three treatment groups (Gem, TMZ, and GC group). 47

1 Introduction

1.1 Glioblastoma multiforme

1.1.1 Definition

The Glioblastoma multiforme (GBM) is a glial tumor of astrocytic origin that is classified as a grade IV glioma according to the World Health Organization (WHO) classification of tumors of the central nervous system (CNS) (1,2). It is highly malignant and grows aggressively in an infiltrating manner, diffusing into neighboring brain tissue, and spreading along myelin pathways whilst invading eloquent areas of the brain (1).

Even though the term "GBM" is obsolete, the name implies the heterogenic appearance of the tumor, as it demonstrates multifarious picture in macrology and histology (1). Although all GBMs share an astrocytic lineage, the heterogenic pathologic presentation resulted in a classification approach lead by light microscopic features and similarities in different stains (3). However, it was soon to be discovered that this classification did not correlate with the prognostic outcome.

With the emergence of genetic analysis, the WHO redefined the classification system for GBM, which now combines histological and immunohistological features with tumor genetics (3).

1.1.2 Classification

According to the 2021 WHO classification of tumors of the CNS, only adult-type diffuse gliomas, isocitrate dehydrogenase (IDH) wildtype, and histone 3 (H3) wildtype are defined as glioblastoma, IDH wildtype (4).

The GBM IDH wildtype is the most common and malignant glioma in adults as it accounts for 45–50% of all primary malignant brain neoplasms (5). It lacks mutations in the *IDH1* or *IDH2* genes and is associated with a worse outcome compared to the IDH-mutant astrocytoma (6).

Rare subtypes of the IDH wildtype GBM include the giant cell glioblastoma, the gliosarcoma and the epithelioid glioblastoma, which are distinguished based on their histological appearance, not only in terms of presenting an astrocytic differentiation but also by

containing different cytological morphologies such as the mesenchymal or glial differentiation (6,7).

Although the cell of origin remains undetermined, studies suggest an array of astrocytic, neural, neuronal, and oligodendrocytic precursor cells (5).

The former IDH-mutant glioblastoma has been reclassified as a CNS WHO grade 4 IDH-mutant astrocytoma (4,5). These grade 4 astrocytomas have a characteristic point mutation in the *IDH1* or *IDH2* genes (6). Although morphological similarities exist between GBM and astrocytomas, their origin, pathogenesis, and behavior differ from each other (4).

IDH-mutant astrocytomas present with different patterns of molecular alterations and lower enzymatic activity of the O^6-methylguanine-DNA-methyltransferase (MGMT) which improves the therapeutic effects of alkylating chemotherapeutic agents such as temozolomide (TMZ) and are associated with a better outcome than IDH-wildtype GBM (2,6).

1.1.3 Epidemiology

The average age-adjusted incidence rate (IR) of GBM varies slightly, ranging from 0.59 to 3.69 per 100,000 persons depending on the country examined, and ranks as the highest IR among malignant tumors of the CNS (2,8).

GBM is highly uncommon in infants, children and adolescents up to 19 years and only constitutes only 3% of all brain and CNS tumors reported among this age group (8), whereby the age at which the first tumor appears differs according to its pathogenetic origin (2). Tumors of primary origin develop later in life with a median age of 64 years at diagnoses, whereas GBMs of secondary origin will most likely be diagnosed at a mean age of 40 years (2).

According to the data from the 2013 Central Brain Tumor Registry of the United States (CBTRUS) report, the incidence of GBM rises with increasing age and peaks at 75–84 years, before it subsequently drastically decreases after the age of 85 years (8).

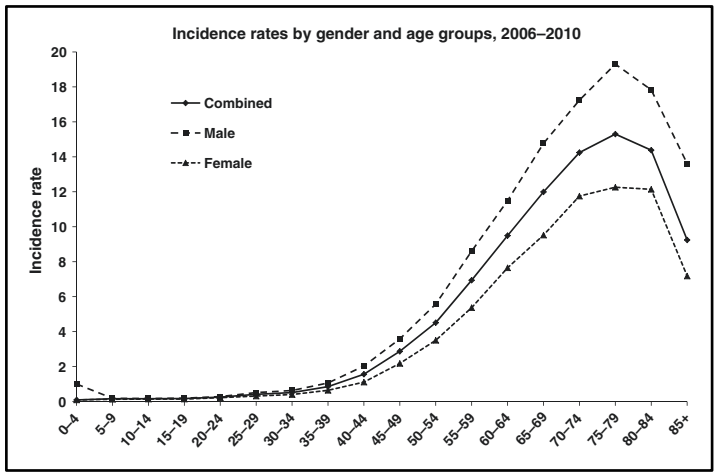

Figure 1. Age and gender-specific IR for GBM, adjusted for age according to the data from the CBTRUS statistical report; reproduced with the permission of the publisher "American Association for Cancer Research"according to license number 1218339-1 (RightsLink®)

Discrepancies in the IRs of GBM between different genders and ethnicities could highlight potential, albeit not yet identified, biological and environmental influences and aspects of its tumorigenesis (8,9).

For instance, in the United States, males have a higher GBM incidence (IR of 3.97 per 100,000 persons) than females, who have an IR of 2.53 per 100,000 persons (2). However, the male-to-female ratio depends on the origin of the tumor. Primary GBMs have a higher IR in men, with a male-to-female-ratio of 1:0.33, whereas the IR of secondary GBMs is higher in females, with a male-to-female-ratio of 0.65:1 (2).

Regarding the prevalence of GBM among different ethnic groups, the white population has the highest IR at 3.45/100,000 population (8).

After evaluating data compilations by CBTRUS, an increase in the incidence of GBM was observed in the time period between 1985 and 1994 (10) and these results initiated a search for different environmental determinants influencing its genesis.

Even though numerous genetic and environmental elements have been studied for their influence on the development of GBM, none of these can conclusively be implicated in several tumors that are observed in practice and most GBM appear to be sporadic (8). While exposure to therapeutic ionizing radiation in early infancy or childhood is one of the known factors for a significantly increased risk of GBM, radiation used in diagnostics, such as X-Rays, has not been linked to a higher risk of GBM (10).

Furthermore, hereditary tumor syndromes such as Li-Fraumeni syndrome and Turcot syndrome are currently the only confirmed genetic predispositions for GBM (2).

1.1.4 Pathogenesis

The genetic composition of GBM is highly heterogenic. However, despite this variety in genetic mutations, three main molecular genetic pathways of tumor origin have been identified and can coexist within the same tumor (2). These pathways determine the presence of oncogenetic factors and signaling pathways in the tumor, resulting in the invading tendencies, growth, and overall aggressiveness of the neoplasm that limit the positive outcome for each patient.

As some molecular genetic pathways are unique to their tumor classification – even if no histological differences between tumors are noticeable – the improvement of molecular diagnostics and its integration into the diagnostic process has helped to more accurately ascertain a given prognosis (6).

In the healthy cell, mitogens bind on cell membrane receptors to trigger an intracellular signaling cascade stimulating cell proliferation and cell growth (11). Receptor tyrosine kinases (RTK) are a large family of transmembrane growth factor receptor proteins which bind growth-promoting ligands such as epidermal growth factor (EGF), vascular endothelial growth factor (VEGF), and platelet-derived growth factor (PDGF) (6).

The hyperactivation or mutation of RTKs leads to disproportionate proliferation, growth, stimulation, and cell division in GBM cells (11,12). The RTK epidermal growth factor receptor (EGFR) is amplified in approximately 40% of GBMs (5), whereby EGFRvIII is the most common EGFR mutation which is found in 20–30% of GBM cases and causes deletion of exons 2–7 (2,11). With the deletion of these alleles, the receptor loses its dependency on ligand stimulation and shifts into a consecutively active state (2). The severe dysregulation and reduced dependence on exogenous growth stimulation results in the characteristic rapid and invasive growth of the tumor (11).

The phosphatidylinositol-3-OH-kinase (PI3K)/AKT/mTor-pathway is part of the EGFR-triggered downstream signaling cascade and its activation influences cell growth and proliferation, and inhibits apoptosis (13). The phosphatase and tensin homolog (PTEN) acts as its main antagonist, as it inhibits further downstream signaling (5,13). PI3K pathway genes and PTEN are alterated in approximately 90% of GBM cases (5).

P53 is a tumor suppressor protein that operates as a transcription factor regulating the promoters of over 2,500 effector genes (11). It occupies a key role in cell cycle control and inhibits the propagation of cells with damaged deoxyribonucleic acid (DNA) (2). If the physiological cell encounters extrinsic or intrinsic stress factors, such as ultraviolet (UV) rays, gamma radiation, or oxidative free radicals, DNA damage occurs which triggers a well-measured response from p53 (14). This response ranges from G1 cell cycle arrest and inducing repair enzymes to apoptosis of the damaged cell (14). In glioma pathogenesis, genetic dysregulation and the consequent loss of p53 function occur in approximately 90% of GBM (5), whereby the inactivation of p53 results in the continuous proliferation of damaged cells with unstable genomes (11).

The retinoblastoma (RB) pathway is essentially universally altered in all gliomas, although it is not the sole contributor to gliomagenesis (11). In non-proliferating cells, hypophsphorylated RB binds and inhibits the E2F transcription factor, which inhibits genes promoting cell cycle and DNA transcription (2). Mitogenic stimulation induces enzymes to phosphorylate RB, releasing E2K which in turn transactivates imperative genes for cell cycle progression from the G1 to S phase and DNA replication (2,5). By means of different genetic mutations culminating in methylation of the RB promotor, glioma cells circumvent the RB-mediated cell cycle barrier causing disruptions in the cell cycle (2). The unimpeded tumor cell continues its G1-S-progression, which ends in the replication of mutated DNA and pathological cell proliferation.

Although the highlighted pathways and their role in tumorigenesis are well known, their full impact on gliomagenesis is complex and yet to be explored.

Consistent with the heterogeneity of GBM tumors, the variability of the occurrence of the mutagenetic pathways differs in each individual tumor lesion and intratumoral progression (2). This diversity allows the tumor to react to extrinsic selective pressure and leads to heightened resistance to radiotherapy and chemotherapy (2,11).

1.1.5 MGMT promoter status

The activity of the DNA repair enzyme MGMT directly influences a tumor's resistance to alkylating therapeutic agents (5), which induce cytotoxicity by adding alkyl groups to DNA bases, and subsequently generating N^7-methylguanine, N^3-methyladenine, and the highly cytotoxic O^6-methylguanine (6,15). Additionally, bifunctional alkylating agents induce the

formation of DNA-crosslinks (16). These crosslink impede the normal uncoiling of DNA strands during tumor cell division, resulting in a potent cytotoxic effect (16). Both mechanisms are a substantial trigger for cytotoxicity and induce apoptosis (6,15,16). Prominent examples of alkylating agents used in the treatment of GBM include systemically administered TMZ and carmustine, which is locally applied in the form of implanted soaked wafers (6,17).

MGMT is a DNA repair enzyme that reverses the chemotherapeutic effect by specifically transferring the methyl group, thereby restoring the original DNA structure with its functional bases and irreversibly inactivating itself in the process (6,17). Through this mechanism, MGMT manifests its importance in the resistance of GBM cells to alkylating agents. Although this process is not definitively characterized, and other proteins are also associated with TMZ resistance, MGMT activity (or the lack thereof) correlates with the response of GBM cells to alkylating chemotherapeutic agents (17,18). For instance, high MGMT activity is linked to enhanced resistance to alkylating chemotherapeutic drugs (17). The epigenetic transcriptional silencing of MGMT is a genetic deviation in GBM that results in lower MGMT expression in tumor cells (6,17).

Epigenetic transcriptional gene silencing is achieved through hypermethylation of the CpG-island, which acts as the promotor regions of MGMT transcription (6). As MGMT irreversibly inactivates itself after the transfer of alkyl groups, constant *de novo* synthesis is needed to maintain MGMT function (17) and hence MGMT promotor methylation is a predictive parameter of the benefit of alkylating chemotherapy (5). The methylation of CpG-promotor-islands is more common in IDH-mutant gliomas than in IDH-wildtype glioblastomas (5).

In the diagnostic process, the MGMT activity is either determined using a polymerase chain reaction (PCR) or an immunohistochemical assay (17).

1.1.6 Pathology

Despite the incorporation of recent advances in genetic and molecular diagnostics, the traditional macrological and histological pathology of glioblastoma is still a central component in diagnostics (19). The macroscopic appearance of GBM is characterized by its rapid, diffuse, and infiltrative growth (8). These attributes contribute to large lesions that are commonly unilateral can cross over the corpus callosum and form a bilateral tumor

manifestation termed butterfly glioblastoma (5). Due to their infiltrating nature, GBM lesions appear poorly delineated against healthy brain tissue (5).

The heterogeneity of the tumor is clearly observed when it is displayed in cross-section, as the cut surface features yellow necrotic tissue in central areas, gray and pink live tumor tissue on the periphery, and red-brown colored foci due to intratumoral hemorrhage (5,8).

Although GBM lesions are generally intraparenchymal-localized single lesions, multifocal lesions have also been reported (5).

GBM presents multiple histological elements, and it is highly cellular, featuring pleomorphic, poorly differentiated tumor cells of astrocytic origin (5,8). The dedifferentiation leads to a wide variety of cellular morphologies, such as undifferentiated, pleomorphic, sarcomatous, or lipidized cells with nuclear atypia and rapid mitotic activity (19). Tumor-induced neovascularization and microvascularization are essential patterns for GBM diagnoses (8,19) and the growth of abnormal blood vessels is generally the reason for the intratumoral hemorrhaging mentioned earlier (5,19). In this context, the typical array of histological features is a necrotic tumor center surrounded by densely cellulated and highly vascularized margins (5,8,19).

Necrosis in GBM can be attributed to several mechanisms, with the key one involving the rapid growth of blood vessels within the tumor (5). These vessels have poorly developed luminal surfaces, rendering them susceptible to clot formation (5). This situation is further exacerbated by the tumor's release of pro-coagulation molecules into the bloodstream (5). As a result, thrombosis occurs, leading to the death of surrounding tissue (5). This creates a harsh microenvironment characterized by acidity, low oxygen levels and glucose deficiency, prompting nearby GBM cells to migrate away from these unfavorable conditions (5).

1.1.7 Outcome and prognosis

As outlined in the preceding sub-chapters, GBM is an extremely aggressive tumor with a very poor prognosis. In the absence of treatment, the median post-diagnosis survival period amounts to only 3 months (20). Tumor treatment, consisting of surgical resection, radiation, and chemotherapy has significantly improved the overall relative survival period to a (admittedly still low) median survival of 15 months (8). The prognosis and treatment options vary on a case-by-case basis, as variables such as age, Karnofsky-Score, tumor location, and tumor characteristics need to be individually ascertained for each patient (8). The long-term

survival status is defined by a post-diagnostic time period of 2.5 years and fewer than 5% of patients achieve a 5-year survival after diagnosis (8).

1.1.8 Clinical presentation

Because of the rapid proliferation of GBM, most patients have a short clinical history with a rapid onset of symptoms within weeks up to 6 months (21). The clinical symptoms largely depend on the localization of the lesion and an early diagnosis is further impeded by the unspecific clinical presentation (5,22).

As the skull presents a spatially limited environment, the expanding tumor mass and the surrounding edematous tissue lead to elevated intracranial pressure (ICP) (21). These pathological shifts cause unilateral localized headaches with an ungeneralized pain pattern that progresses in severity as the tumor expands (21), while additional symptoms of elevated ICP include nausea and vomiting (5). Another mechanism of the expanding tumor tissue is the direct destruction of healthy brain tissue due to necrosis, whereby the loss of tissue presents as a focal neural deficit and cognitive impairments (21). These impairments vary in their clinical presentation depending on the localization and size of the lesion and the possible focal neurological deficits include hemiparesis, visual impairment, loss of hearing, and sudden, profound changes in personality and behavior (5,22). The destruction of healthy brain tissue may also cause newly onset focal or general seizures in adults (21,22). Moreover, the neurological symptoms generally progress in terms of their severity as the tumor increases in size (5).

1.1.9 Current treatment approaches

The current gold standard in GBM treatment is, if possible, maximal safe surgical resection followed by simultaneously applied oral chemotherapy with TMZ and fractioned field radiation therapy (19). The treatment of symptoms such as seizures, cerebral edema, and cognitive dysfunction enhances and rounds off the optimal medical management approach (23). At present, all GBM treatments mentioned are not curative but serve to prolong life, lengthen the progression-free survival period, increase overall survival, reduce symptoms, and improve quality of life (24).

Surgical resection of the tumor mass serves multiple purposes in GBM therapy as it alleviates mass effects and lowers the ICP (6,24). Additionally, surgery provides a sufficient amount of tumorous tissue to conduct the necessary histological and molecular diagnostics

(25). One of the most prominent factors for increased survival is safe maximal surgical resection of the tumor to keep the residual tumor volume as low as possible (24,25) and cytoreductive surgery to decrease the tumor volume by over 98% is associated with an increased survival time of up to 11 to 12 months (26). Furthermore, even if maximal surgical resection is not achievable, submaximal resection is still beneficial to relieve mass effects and ICP (26). However, due to the diffuse infiltration of tumor cells, the extent of surgical resection is restricted as the preservation of neurological function takes priority over radical surgical resection (27).

Between 3 and 5 weeks after surgery, focal radiotherapy with concomitant and adjuvant chemotherapy should be administered (23,27), whereby the delay between interventions allows adequate wound healing (26). The standard external-beam radiotherapy administers fractions of 1.8–2 Gy daily for 5 days per week over the course of 6 weeks, accumulating to yield an overall radiation dose of 50–60 Gy (6,27).

Current cytotoxic chemotherapy options include the alkylating agents TMZ and nitrosurea compounds such as carmustine or lomustine (23,27).

A combination of chemotherapeutical agents is used with the combined chemotherapy of procarbazine, lomustine and vincristine (23).

Due to its excellent ability to penetrate the blood-brain-barrier (BBB), systemic TMZ-chemotherapy is currently the standard of care (2,23).

Gliadel wafers represent a topically applied chemotherapeutical treatment option in which the biodegradable carmustine depot is implanted into the cavity after surgical tumor resection and releases carmustine for approximately 3 weeks (23). Even though some studies show a slight survival benefit, Gliadel wafers are only seldom used, as complications such as hematological toxicity, seizures, intracranial edema, and intracranial infections have been reported in conjunction with their use in GBM patients (23,28).

Due to the diffuse infiltration of tumor cells in the neighboring tissue, GBM generally reoccurs after resection within 6.9 months after initial diagnosis (23).

A newly available treatment approach for GBM patients is the use of tumor treating fields (TTF) (27,29). TTF therapy achieves its effect by repositioning the tubulin dimers further from the growing ends of microtubules, therefore disrupting the normal polymerization and depolymerization process of microtubules within the mitotic spindle (29). This leads to the interference of mitosis, causing mitotic catastrophe and, ultimately, cell death (29). This

therapy is typically offered after combined radio-chemotherapy with concurrent maintenance therapy using TMZ (27,29).

The application and integration of newly developed technological treatment options into clinical practice, such as TTF, and the rapid technological advancement open up new avenues for GBM therapy. These advancements underscore the need for complementary developments in the realm of delivery systems, like the organic electronic ionic pump (OEIP). The OEIP's capacity to expand the range of available chemotherapeutic drugs and precisely administer them positions it to address the unique challenges inherent in GBM therapy, ultimately propelling advancements in the field of neuro-oncology.

1.2 Organic electronic ionic pumps

The OEIP belongs to the group of organic bioelectronics that combine electronic and ionic properties in their function (30). This miniature device has both electronic and ionic capabilities, which effectively enables it to translate technological signals into biological ones (30,31). It converts applied electric currents into ionic currents via electrophoresis, as it uses ions (drug molecules) as charge carriers instead of electrons (31). The OEIP is composed of a drug reservoir and a miniaturized glass fiber capillary containing a polymeric membrane acting as an ion channel (32). This membrane thus acts as an cation or anion exchange membrane (CEM or AEM) (33). In the OEIP used for this study, the CEM is comprised of 2-acrylamido-2-methylpropane sulfonic acid and enables selective electrophoretic transport of charged molecules if electric current is applied, whereby the applied electric current directly correlates to the ionic current of the pump which facilitates exact dosage control (33). Continuous drug delivery steepens the concentration gradient of drug molecules at the release site, which subsequently diffuses into the surrounding tissue (31).

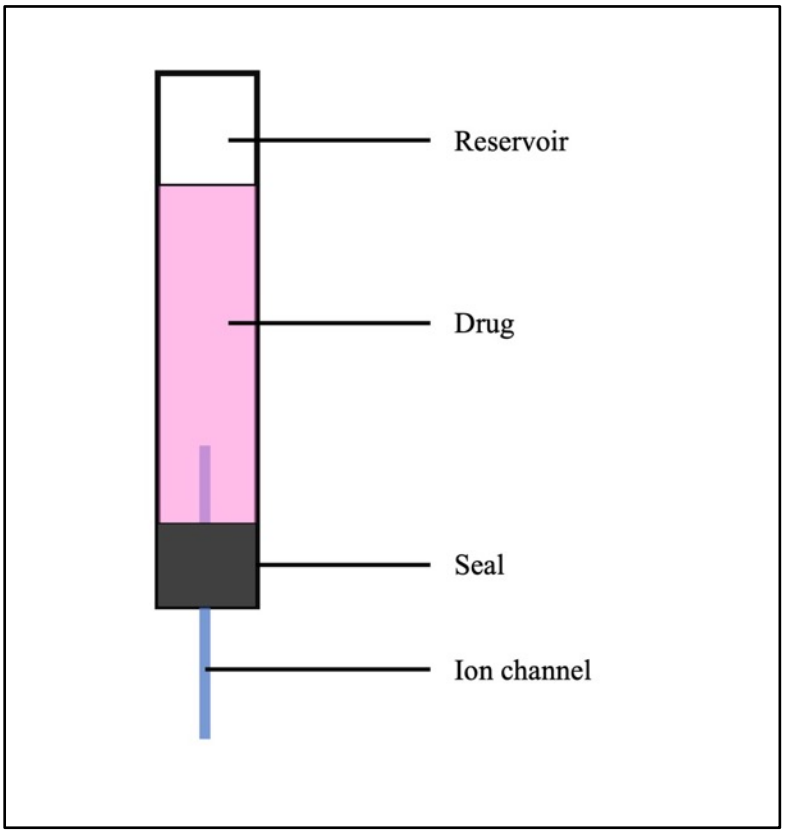

Figure 2. Schematic representation of an OEIP filled with drug. As an electric current is applied, the drug molecules travel through the channel via electrophoresis to their target site.

The OEIP drug delivery approach facilitates high delivery precision at the intended target site with high spatiotemporal resolution (31). It solely delivers the transported ions and forgoes the necessity of solvent solutions, which greatly reduces adverse effects on brain tissue (31,33). As electrophoretic drug delivery does not require liquid flow, this method does not create any interference in spatially limited environments such as the skull (32).

OEIPs have already been used for the delivery of neurotransmitters in both *in vitro* and *in vivo* experiments (30,34) and they have also been applied to interact with and modulate the biochemical regulation system of plants (35). Furthermore, *in vitro* applications to moderate inflammatory processes were also successfully demonstrated using this approach (36). Most importantly, OEIPs have already demonstrated successful delivery of Gem to GBM cells in *in vitro* conditions (33). The optimization of the OEIP for medical applications in humans could thus incorporate current technological advances and expand treatment options.

1.3 Temozolomide

The alkylating drug TMZ is an imidazotetrazine derivate and is used for systemic chemotherapy in GBM and high-grade astrocytomas (18). Because of its lipophilic nature, TMZ is able to cross the BBB, which enables oral administration (18). TMZ is a prodrug that is stable at an acidic pH, but is rapidly hydrolyzed to its active form 5-(3-methyltriazen-1-yl) imidazole-4-carboxamide (MTIC) at a pH above 7 (18). MTIC is further hydrolyzed to methyldiazonium ions which damage DNA (37). The cytotoxic effect of TMZ occurs by the methylation of guanines at N^7 and O^6 and adenines at O^3 in DNA, whereby the resulting DNA damage leads to cell cycle arrest at G2/M and apoptosis (18).

1.3.1 Resistance of glioblastoma cells against temozolomide

The development of TMZ resistance in GBM cells is multifactorial and arises through complex interactions of various molecular mechanisms (37). Due to the mutagenetic nature of GBM cells, the development of TMZ resistance is quite common and as many as 50% of patients do not respond to chemotherapy with TMZ (37). This matter is further complicated by the fact that TMZ resistance can either be acquired within the first treatment regimen or be an inherent feature of the tumor cells (37). One of the primary causes of TMZ resistance is thought to be the result of glioma stem cells (GSCs) (37). Although GSCs only amount to only 1% of tumor cells, their undifferentiated, tumorigenic nature and their capability to symmetrically divide into daughter cells results in the ability of self-renewal of the tumor and tumor progression (38). Mapping studies and genome and exome sequencing of recurrent GBMs have shown that chemotherapy places selective pressure on GSCs which increases TMZ-resistant GSCs (37). In this context, it is presumed that the applied selective pressure produces GSCs with an upregulation of DNA repair mechanisms, such as heightened MGMT expression, in conjunction with augmented expression of enzymes for base excision repair and mismatch repair (37). The hyperactivated or mutated key molecular pathways that are mentioned in Chapter 1.1.4. further contribute to TMZ resistance (37).

1.4 Gemcitabine

Gem is an approved chemotherapeutic drug for the treatment of various solid tumors such as pancreatic cancer, non-small-cell lung cancer, and breast and ovarian cancer (39). It is a nucleoside analogue and shares structural similarities to cytidine, whereby the cytotoxic impact of Gem is achieved through MGMT-independent mechanisms (39).

Administered as a prodrug, Gem is sequentially phosphorylated to Gem-monophosphate, Gem-diphosphate and finally to its active metabolite, Gem-triphosphate (39). Another metabolic conversion of Gem through cytidine deaminase results in the formation of 2',2'-difluorodeoxyuridine (dFdU) (39). Gem-triphosphate competes against deoxycytidine-triphosphate and is incorporated into DNA during replication (39). Its integration leads to the irreversible inhibition of DNA polymerases and further blocks DNA chain elongation, whereby the resulting DNA fragments induce cell death by apoptosis (39).

Additionally, Gem-diphosphate functions as an inhibitor for ribonucleotide reductase, an enzyme involved in DNA synthesis (39). This action creates a self-potentiating effect of Gem as it diminishes the production of deoxyribonucleoside-triphosphate precursors, which decreases the levels of deoxycytidine-triphosphate and deoxyadenosine-triphosphate (39).

Even with short exposure durations, Gem features potent radiation sensitization properties at noncytotoxic drug levels (39). The Gem metabolite dFdU also exhibits radio-sensitizing effects and additionally displays cytotoxic effects at easily attainable plasma concentrations (39). Although the exact underlying mechanism of Gem's radio-sensitizing ability is not yet fully elucidated, it is thought that the depletion of phosphorylated deoxynucleotides such as deoxyadenosine-triphosphate and the drug-induced cell-cycle shift into the S-phase are key contributing factors (39).

Even though the cytotoxic and antitumorigenic effect of Gem on GBM cell lines has already been established *in vitro* by Rieger et al. (40), the clinical use of Gem for GBM has been impeded due to limitations resulting from its short-term plasma half-life, side effects at systemic high-dose administration (systemic toxicity), and low penetration of the BBB (39,40).

To enhance the effectiveness of Gem against GBM, the application of a localized delivery approach such as OEIPs may circumvent the constraints associated with systemic toxicity and enable the administration of higher drug concentrations to the target site.

1.5 Chicken chorioallantoic membrane assay

The development and establishment of a new clinical treatment approach necessitates comprehensive research, including both *in vitro* and *in vivo* testing. While many *in vivo* studies rely on transgenic mice, these models are costly and intricate, often presenting challenges in obtaining morphological data. The CAM assay serves as a dependable alternative, offering a well-established *in vivo* environment for drug screening prior to implementing expensive, more complicated, and lengthy animal models (41,42). In Austria, an ethics committee's approval is not needed to employ a CAM model. The CAM assay has been established as a reliable model in different research fields, including but not limited to cancer research, bioengineering, and transplant biology (43).

The membrane develops extra-embryonically and provides a highly vascularized structure consisting of two epithelial layers that enclose a stromal layer, whereby the vascular and lymphatic vessels lie within the stroma (43). *In ovo*, the membrane adheres to the surface of the eggshell, extracting calcium from the shell and acquiring oxygen for the avian embryo through the permeable surface (43). The highly vascularized environment provided by the membrane and the ability to accommodate grafts of foreign tissue makes the CAM assay an appealing *in vivo* model for pharmaceutical testing (44). As the membrane attaches to the shell after 4 days of embryonic development, the process of cracking the eggshell for *ex ovo* cultivation therefore needs to occur on day 3 (43).

2 Aims of this study

Given the pressing need for novel GBM treatment options, the collaborative efforts of Linda Waldherr, M.Sc., Ph.D., and Assoc. Prof. Priv.-Doz. Dipl.-Ing. Dr. techn. Rainer Schindl from the Institute of Medical Physics and Biophysics of the Medical University of Graz and Professor Daniel Simon, Ph.D., from Linköping University, are dedicated to the development of an OEIP designed to enable precise localized drug delivery for an innovative approach to local treatment.

The aim of this thesis was to conduct preliminary studies and pilot experiments to support the advancement of the aforementioned OEIP.

Given Gem's alignment with the chemical prerequisites of the OEIP, this study aimed to verify Gem's anti-neoplastic impact on GBM cells relative to the established gold standard of chemotherapy with TMZ, under both *in vitro* and *in vivo* conditions.

3 Materials und Methods

To assess the anti-tumor efficacy of Gem relative to TMZ, a comparative *in vitro* analysis of tumor cell proliferation was conducted. For this purpose, three different GBM cell lines (A-172, LN-18 and U-251) were treated with varying concentrations of Gem and TMZ, and their impact on tumor cell proliferation was evaluated with a CellTiter 96® AQ_{ueous} Non-Radioactive Cell Proliferation (MTS) Assay (Promega, USA).

To further determine Gem's anti-tumor efficacy on tumor growth, an *in vivo* CAM model was used to emulate a 3D tumor of LN-18 cells, and CAM-cultivated tumors were treated with Gem and TMZ at different drug concentrations. The impact of drug treatment on tumor growth, solidity, and viability was measured using immunohistological staining (Ki-67) and bioimage analysis read-outs via QuPath software.

3.1 Cell lines

To investigate the anti-tumor efficacy of Gem relative to TMZ, three established human glioblastoma cell lines, namely A-172, LN-18, and U-251 MG, were used.

A-172 is a patient-derived human glioblastoma cell line obtained from the cell culture facility of the Medical University of Graz which was cultured in Dulbecco's Modified Eagle's Medium (D-MEM) supplemented with 2 mM L-Glutamine and 10% fetal bovine serum (FBS) at 37°C and 5% CO_2.

LN-18 (ATCC® CRL2610™) is a human glioblastoma cell line derived from a 65-year-old male patient with GBM in the right temporal lobe. For cell culture, we used D-MEM supplemented with 5% FBS at 37°C and 5% CO_2.

U-251 MG is a cell line from the cell culture facility of the Medical University of Graz derived from a GBM patient and was cultivated in D-MEM supplemented with 10% FBS and 2 mM L-glutamine, maintained in an environment of 37°C and 5% CO_2.

Table 1. Properties and information concerning the GBM cell lines employed

	A-172	**U-251 MG**	**LN-18**
Organism	*Homo sapiens* (human)	*Homo sapiens* (human)	*Homo sapiens* (human)

Tissue	Brain	Brain	Brain/cerebrum, right temporal lobe
Cell type	Glioblastoma	Neuronal cells	Glioblastoma (grade IV)
Morphology	Epithelial	Pleomorphic/ astrocytoid	Epithelial
Growth Properties	Monolayer, adherent	Monolayer, adherent	Adherent

3.2 Cell culture

All cell culture media and supplements utilized were procured from Thermo Fisher Scientific, USA. The cell lines of interest were cultivated in T75 tissue flasks equipped with a canted neck and a red cap. To ensure a fresh supply of nutrients for the tumor cells, the cell culture medium was regularly replaced while cell splitting was used to sustain the exponential growth of the cells. The splitting ratio and splitting frequency were adjusted to meet the specific requirements of each cell line depending on the individual growth rate of the cell lines used.

Table 2. Growth rate, splitting ratio and splitting frequency in the three GBM cell lines.

	A-172	**U-251 MG**	**LN-18**
Growth rate (observed)	slow	fast	normal
Splitting ratio	1:4	1:10	1:10
Splitting frequency	1x/week	2x/week	1-2x/week

The cell harvesting process commenced by removing the existing cell culture medium from the T75 flasks after which the cells were gently flushed with phosphate buffer saline (PBS). Afterward, 1–2 mL trypsin was added to the cells before they were stored in an incubator at 37 °C and 5% CO_2 for 1 minute until the cells started detaching from the flask in the visual control under the microscope. After the cells were detached from the flask, 7 mL of cell culture medium was added to the flask to rinse the cells, and the cells and medium were

subsequently transferred into a falcon tube and centrifugated for 5 minutes (min) at 500 rpm at room temperature (RT). The excess medium was removed from the falcon tube and a defined amount of medium was readded to the cell pellet before the medium and the cell pellet were gently blended. The number of cells was determined through cell counting using the Luna-II™ Automated Cell Counter (Logos Biosystems, South Korea), whereby the volume of the cell suspension needed to obtain the required quantity of cells was calculated with the following equation:

$$\frac{needed\ amount\ of\ cells\ per\ well\ \times\ number\ of\ wells}{number\ of\ counted\ cells\ [mL]} = volume\ needed\ [mL]$$

The calculated volume was extracted from the flask for further treatment, and the excess of cells were transferred to a new T75 cell culture flask with 10 mL of fresh medium.

3.3 IC_{50} determination

To directly compare the anti-tumor potency of Gem and TMZ chemotherapeutic agents, the IC_{50} curves for both substances were determined. To ascertain the IC_{50} value for Gem and TMZ, the different cell lines (A-172, LN-18 and U-251 MG) were treated with a range of concentrations of both chemotherapeutic agents for 72 h alongside an untreated growth control (GC) for comparison.

3.3.1 Experimental setup for IC_{50} determination

The harvested cells were dispersed in the required volume of medium (200 µL medium/well) and in the final step distributed in a flat-bottomed 96-well plate (Corning, USA). Cell lines A-172 and LN-18 were seeded with 4,000 cells per well in 200 µL medium per well, whereas due to the rapid proliferation rate observed in U-251 MG, a cell count of 1,500 cells per well was used for this particular cell line. Following cell seeding, the cells were incubated at 37 °C and 5% CO_2 for 24 h to allow them to settle in the well plate. After 24 h, the medium in the wells was carefully removed and replaced with an equal volume of medium containing varying concentrations of Gem or TMZ. The treatments duration was 72 h.

TMZ was stored as a dry powder at 4 °C. Just before use, it was weighed and dissolved in the specific medium of the cell lines used. TMZ was diluted with medium into the following

concentrations: 50, 100, 500, 1,000, 2,000, 5,000, 7,000 and 10,000 µM. Three wells were allotted per concentration, while three additional wells were designated for the untreated GC that only received fresh medium. The cells were treated for 72 hours in an incubator at 37 °C and 5% CO_2.

For Gem, concentrations of 0.0001, 0.001, 0.01, 0.1, 1, 5, 10, 50 and 100 µM were used. The Gem stock solution with a concentration of 10 mM (Cayman Chemical Company, 11690) was stored at -20°C prior to use and was subsequently diluted into the cell-specific medium according to the dilution pattern outlined above. Three wells were allotted per concentration and an additional untreated GC group was added. The cells were treated for 72 hours in an incubator at 37 °C and 5% CO_2.

3.3.2 MTS assay

The MTS assay was used to measure the proliferation rate of viable tumor cells. This assay consists of a tetrazolium compound and an electron coupling reagent and viable, metabolically active cells bioreduce this compound into a formazan product via dehydrogenase enzymes. The soluble formazan product can be measured at an absorbance of 490 nm and is directly proportional to the number of viable cells in the culture.

The assay was performed according to the manufacturer's protocol and the read-outs were conducted using a CLARIOstar plate reader (BMG, Labtech, Germany).

The initial read-out occurred after 1 h of incubation with MTS, while the second read-out took place after a 2 h incubation period at 37 °C and 5% CO_2.

3.3.3 Statistical analysis of the IC_{50} values

To ensure accurate determination of cell viability, the raw data was blank corrected (bc) by subtracting the values from a media-filled well to eliminate any potential influence of the media on the determined optical density. Each well generated one data point. The cell viability in each well was calculated using the following equation:

$$cell\ viability\ (\%) = \frac{(bc\ data\ point)}{mean\ of\ bc\ control\ group} \times 100$$

The IC_{50} value was determined using the equation below, whereby the minimum (Min) and the maximum (Max) refer to the minimally and maximally inhibited responses:

$$Y = Min + \frac{Max - Min}{1 + (\frac{X}{IC50})^{Hill\ coefficient}}$$

All data points were plotted as a mean ± standard deviation (SD) using Prism GraphPad software.

3.4 Preparation for the CAM assay

Upon delivery (day 0), the fertilized eggs underwent a careful cleansing process using tepid water (20 °C) and a soft brush to eliminate dirt or impurities, followed by disinfection using 75% ethanol. The eggs were subsequently placed in an incubator (37.6 °C, humidity level 40–60%) for 3 days.

On the third day of incubation, the eggs were prepared for *ex ovo* cultivation. The predetermined breaking point was first disinfected with 75% ethanol, after which the shell was broken using an electrical blade. Subsequently, the contents of the eggs were carefully transferred to a sterilized plastic Petri dish that was promptly covered with a plastic lid to avoid contamination.

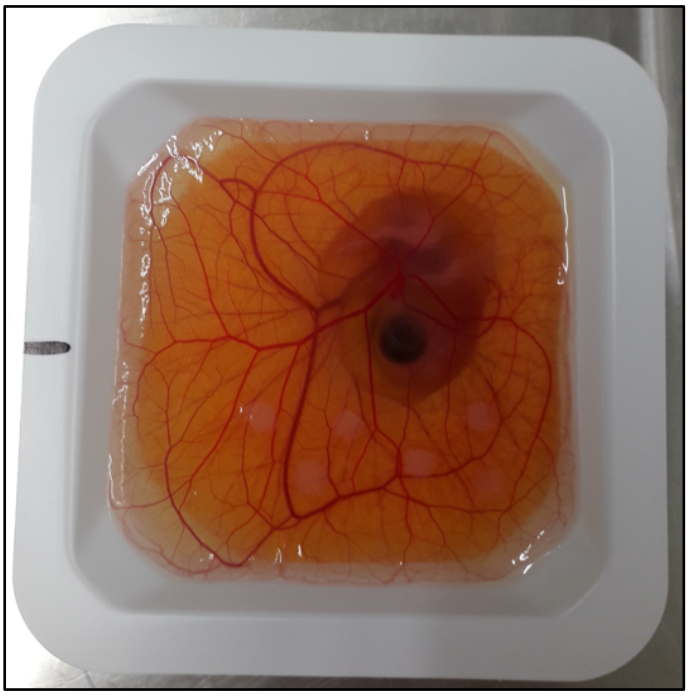

Figure 3. Chicken embryo *ex ovo* (day 10 of development) (property of Manuela Pirker, M.Sc., and used with permission)

In preparation for further experimentation, the contents of the eggs were further incubated under the previous conditions (37.6 °C, humidity level 40–60%) for an additional 7 days.

3.4.1 LN-18 cultivation on CAM

The LN-18 cell line was used for the CAM assay and the experimental setup consisted of three treatment conditions: Gem, TMZ, and GC. The drug concentrations used, determined by the previously derived IC_{50} curves, were 100 µM for Gem and 1.5 mM for TMZ. The GC group did not receive any treatment. Each onplant contained 10^6 cells and the experiment was repeated three times. It should be noted that some embryos died under incubation conditions and such cases are marked with a cross symbol (†).

Table 3. Setup of CAM assay #169 with LN-18 and three treatment conditions

CAM #169	**Gem 100 µM**	**TMZ 1.5 mM**	**GC**
Cell count/onplant	1 x 10^6 cells	1 x 10^6 cells	1 x 10^6 cells
Onplants/egg	2	2	2
eggs/condition	4 2	3 2	3 0

- embryos perished (†)			
Total amount of onplants/condition	8	6	6
CAM assay number	#132 † #136 † #139 #142	#133 † #137 #140 †	#134 #138 #141

Table 4. Setup of CAM assay #174 with LN18 and three treatment conditions

CAM #174	**Gem 100 µM**	**TMZ 1.5 mM**	**GC**
Cell count/onplant	1 x 10^6 cells	1 x 10^6 cells	1 x 10^6 cells
Onplants/egg	2	2	2
Eggs/condition **- embryos perished (†)**	5 1	5 1	4 1
Total amount of onplants/condition	10	10	8
CAM assay number	#419 #420 #421 #422 † #423	#414 #415 #416 † #417 #418	#424 #425 #426 #427 #428 †

Table 5. Setup of CAM assay #175 with LN-18 and three treatment conditions

CAM #175	**Gem 100 µM**	**TMZ 1.5 mM**	**GC**
Cell count/onplant	1 x 10^6 cells	1 x 10^6 cells	1 x 10^6 cells
Onplants/egg	3	3	3
eggs/condition **- embryos perished (†)**	3 2	3 1	2 1

Total amount of onplants/condition	9	9	6
CAM assay number	#484 † #485 #486 †	#481 #482 #483 †	#487 † #488

3.4.2 Preparation of LN-18 cells for xenografting

For each onplant in the CAM assay, a total volume of 20 µL was required, which consisted of a 15 µL cell suspension containing the precalculated cell count of 10^6 cells.

In CAM assay #169, 5 µL of Matrigel® was added as an additional compound, while in CAM assays #174 and #175, 5 µL of Geltrex™ was used. The combination of Matrigel® or Geltrex™ with medium served as extracellular matrix and ensured nutritional support for the GBM cells until the xenograft could establish a supporting vascular network. The prepared solution was subsequently stored on ice until xenografting, but for a maximum for 15 min.

Table 6. Volume and composition of the cell suspension per onplant. The cell suspension with medium supplied nutrients to the system while the carrier matrix counteracted cell dispersion.

CAM assay	**#169**	**#174**	**#175**
Cell suspension	15 µL	15 µL	15 µL
Carrier matrix	Matrigel®	Geltrex™	Geltrex™
- volume added	5 µL	5 µL	5 µL
Final volume	20 µL	20 µL	20 µL

3.4.3 Xenografting

To xenograft the tumor cell suspension onto the CAM, sterile silicone with a diameter of 5 mm rings were used, with one ring allocated per onplant, and the number of rings placed per egg corresponding to the predetermined number of onplants. Using sterilized surgical tweezers, the rings were carefully positioned on the CAM of each embryo within a bifurcation of smaller blood vessels. Using pre-chilled sterile pipette tips, the prepared cell solution was carefully pipetted into each ring at a volume of 20 µL per ring.

Following the xenografting, the embryos were further cultivated for an additional 24 h at 37.6 °C and 40–60% humidity. This incubation period allowed for the development of solid tumors before subsequent treatment.

3.4.4 Treatment of LN-18 onplants

After the 24 h incubation period, the xenografted cells adhered to the CAM and formed solid tumors. The onplants received blood supply through the newly developed blood vessels of the CAM, which were induced by the tumor growth. The embryos that were no longer viable were removed from the experiment and appropriately discarded. The Gem used was stored as a 10 mM stock solution at -20 °C and diluted to a concentration of 100 µM in medium, while TMZ was stored as a powder at 4 °C and dissolved in Dimethyl sulfoxide (DMSO) to prepare a 50 mM stock solution. This stock solution was further diluted with sterile H_2O (Fresenius Kabi, USA) to obtain a final concentration of 1.5 mM for treatment.

The concentrations of Gem and TMZ used in this assay were based on the previously determined IC_{50} values from the results of the *in vitro* experiments, detailed in Subchapter 4.1 and 4.2. To administer the treatment, 20 µL of the prepared stock solutions were directly pipetted onto each onplant while ensuring that the sterile pipette tip did not come into contact with the tumors or the membrane. The GC group did not receive any treatment. The embryos were then further incubated for 72 h at 37.6 °C and 4040–60% humidity.

3.4.5 Harvest, fixation, and paraffin-embedding of onplants

After 72 h of treatment (on day 13 after fertilization), the xenografts consisting of silicone rings and tumors were carefully excised from the embryos with sterile surgical tweezers and scissors. To minimize bleeding, metabolic activity, and the response of the embryo, the embryos were chilled on ice before excision. Once the xenografts were removed, the chicken embryos were cooled to -20 °C, and the remains were safely disposed of at the carcass disposal site (TKV Graz).

The removed xenograft was placed into a sterile Petri dish containing PBS and subsequently photographed from the top and from the bottom with the Olympus SZX16 stereomicroscope and cellSens software.

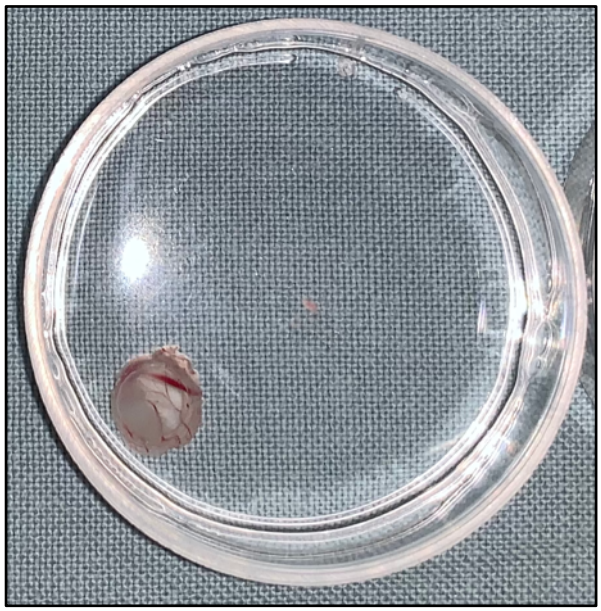

Figure 4. Macroscopic image of the harvested xenograft in a sterile Petri dish containing PBS.

In preparation for the fixation and embedding process, the tumors were individually placed into Petri dishes filled with 4% paraformaldehyde (PFA) for 12 h at RT.

The xenografts were subsequently moved to labeled Tissue-Tek embedding cassettes. To ensure that the tumors remained in position during the embedding procedure, two pieces of laboratory blotting paper measuring 2.5 x 3 cm each were inserted into the cassettes. The embedding process followed the sequence detailed in Table 7.

Table 7. The embedding protocol followed for the paraffinization of the harvested xenografts

Step	Reagent	Percentage	Temperature	Time
1	Ethanol	70%	RT	30 min
2	Ethanol	95%	RT	30 min
3	Ethanol	95%	RT	15 min
4	Ethanol	100%	RT	30 min
5	Ethanol	100%	RT	15 min
6	Toluene			30 min
7	Toluene			15 min
8	paraffin #6		61 °C	40 min
9	Removal of silicone rings			
10	paraffin #9		61 °C	40 min
11	paraffin #9		61 °C	
12	Cooling of paraffin blocks at -15 °C until hardened			

After embedding the xenografts into paraffin, the paraffin blocks were stored at 4 °C.

3.5 Histological analysis

To assess the histological impact of the treatments, the paraffin-embedded tumors needed to be prepared for hematoxylin-eosin (HE) staining. The paraffin blocks were sliced into 5 µM sections using the Leica RM2245 V2.4 rotary microtome (Leica Biosystems Nussloch GmbH) and straightened with a water bath set at 36 °C. The produced sections were gently put onto white-tabbed SuperFrost Plus™ Adhesion Slides (Epredia, USA) and dried on a heating plate at 37 °C for a minimum of 1 hour.

3.5.1 Hematoxylin eosin staining

The HE-staining of the microscopic slides prepared as described in Chapter 3.5 was carried out at RT in a sterile laminar flow hood, following the protocol detailed in Table 8.

Table 8. HE staining protocol

Step	Reagent	Duration	Effect
1	Xylene (1st bath)	3 min	Deparaffinization
2	Xylene (2nd bath)	3 min	Deparaffinization
3	Ethanol 100% (2x)	3 min	Removal of xylene
4	Ethanol 95% (2x)	3 min	
5	Ethanol 70-80% (2x)	3 min	
6	H_2O (distilled)	3 min	Tissue hydration
7	Hematoxylin	2 min	Nuclei staining
8	Rinse in H_2O (cold)	Until water remains clear	Removes excess staining
9	0.5% Acidic ethanol	5 s	Decolorizes background
10	Rinse in H_2O (cold)	3 min	
11	Ammonia water	2-5 min	Until slides have blue shade
12	Rinse in flowing H_2O (cold)	3 min	
13	Ethanol 70-80%	3 min	
14	Eosin	1 min	Staining of acidophilic tissues

15	Ethanol 95% (3x)	1 min each bath	Removal of excess eosin staining
16	Ethanol 100% (2x)	3 min each	
17	Xylene (2x)	3 min each	
18	Cover with mounting media (toluene) and coverslips		Better optical quality

HE-staining results in bright blue nuclei and bright pink cytoplasms on the slides, and the HE-stained slides were subsequently photographed with a stereo microscope (Olympus SZX16) and cellSens software at four different magnifications (4x, 10x, 20x, and 40x). The slides allowed for histological analysis and served as preliminaries to select slides for immunohistochemistry.

3.6 Immunohistochemistry – Ki-67-staining

3.6.1 Ki-67 proliferation index

To determine the proliferation index of the treated tumors, the selected tumor sections were immunohistochemically stained with the Ki-67 protein by Sen. Scientist Dr. med. Univ. Martin Asslaber, Department of Pathology and Molecular Biomedicine, Medical University of Graz.

Immunohistochemical staining for Ki-67 was performed in the automated DAKO OMNIS system with the primary DAKO anti-Ki-67 antibody clone Molecular Immunology Borstel (MIB-1) (GA62661-2) and DAKO OMNIS Flex HRP detection system. All slides were documented with the Nikon Eclipse E400 microscope and Zwo Asi 183 MC pro camera, and brown-stained cells indicated positivity for Ki-67.

3.6.2 Quantification of positive cells with QuPath

To determine the Ki-67 index with the stained slides, the Bioimage Analysis QuPath open-source software was used which features built-in algorithms for cell and tissue detection, and interactive machine learning to detect stained tumor cells (45).

The stained slides were digitalized by scanning each whole slide as a high-resolution image stacked in SVS file format. After the files were imported into QuPath, each tumor was manually marked and the setup parameters were set to “optical density sum.” All parameters that were defined are detailed in Figure 5.

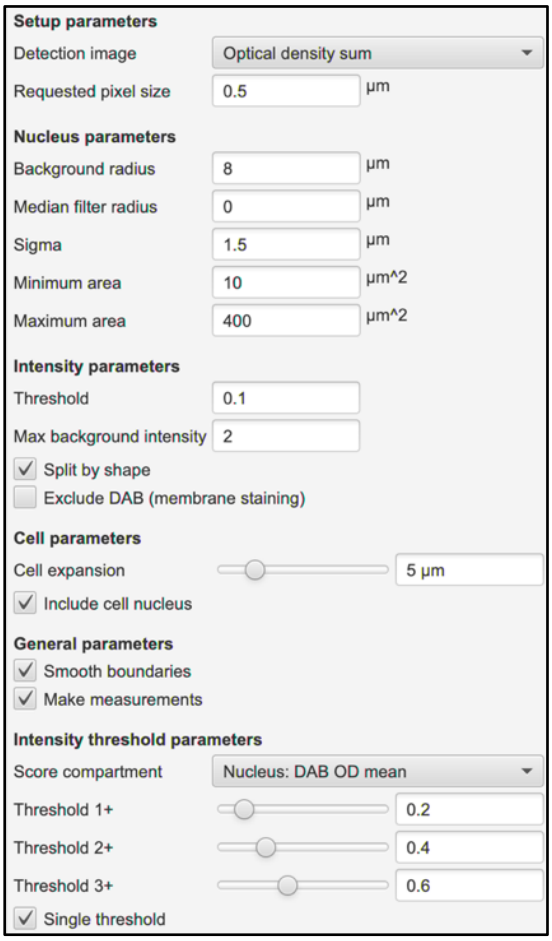

Figure 5. Screenshot of the parameters used for positive cell detection in QuPath.

As the software analyzed the selected tumor using the specified parameters, QuPath conducted a count of all cells in the marked area, including the negative and positive cells together with the total number of cells. Subsequently, the index was calculated by dividing the count of positive cells detected by the total number of cells assessed.

To generate high-resolution images, the CaseViewer software was used to open and convert the SVS file format into JPEG format and all digitalized slides were saved, cataloged, and stored on a local hard drive.

3.6.3 Statistical analysis of Ki-67 indexes

For the statistical analysis, all collected data was categorized into treatment groups (Gem, TMZ, and untreated) and analyzed using IBM SPSS Statistics 28 and JASP 0.17.2.1 (Apple Silicon) software (46).

To ascertain the presence of a normal distribution within the gathered dataset, an assessment was conducted using Shapiro-Wilk test. Subsequently, an outlier analysis was performed

and the Shapiro-Wilk test was repeated. To check the homogeneity of variances, Levene's test was performed. The statistical analysis was performed employing the Kruskal-Wallis test to establish the statistical significance of the findings. Additionally, all collected data was graphically presented for a comprehensive overview in Figure 17 using Prism GraphPad software.

4 Results

This study compared the efficacy of chemotherapeutic treatment with Gem and TMZ on three different GBM cell lines (A-172, LN-18 and U-251 MG) *in vitro*. Additionally, the effects of Gem and TMZ were tested *in vivo* using the CAM assay methods.

4.1 IC_{50} curves of TMZ

As outlined in Chapter 3.3.1, each well contained 4,000 cells for cell lines A-172 and LN-18, and 1,500 cells for cell line U-251 MG. The cells received a single treatment with TMZ in increasing drug concentrations. After treatment, the cells were incubated for 72 h and subsequently assessed for their proliferation rate with the MTS assay. The procedure was repeated twice for cell line A-172, with a total sample size of n = 6 for each concentration and once for U-251 MG and LN-18 with a sample size of n = 3 for each concentration in these cell lines. The results in all three cell lines show the continuous decrease of mean cell viability as the TMZ concentration increased, and the IC_{50} values determined are shown in table 12.

Table 9. Mean cell viability (%) and SD in GBM cell line LN-18 after 72 h of treatment with different TMZ concentrations. N = 3 for each concentration in one experimental run.

TMZ concentration (µM)	Mean cell viability (%)	SD (%)
0	100	5
50	100	8
100	92	10
500	84	6
1000	59	7
2000	48	2
5000	23	2
7000	16	10
10000	20	8
12500	23	6
15000	16	4
20000	14	4

Table 10. Mean cell viability (%) and SD in GBM cell line A-172 after 72 h of treatment with varying TMZ concentrations. N = 6 from two independent experiments.

TMZ concentration (µM)	mean cell viability (%)	SD (%)
0	100	0
50	88	22
100	72	30
500	75	42
1000	78	14
2000	45	36
5000	37	20
7000	7	7
10000	18	18

Table 11. Mean cell viability (%) and SD in GBM cell line U-251 MG after 72 h of treatment with varying TMZ concentrations (µM). N = 3 in one experimental run.

TMZ concentration (µM)	mean cell viability (%)	SD (%)
0	100	35
50	77	22
100	89	13
500	117	32
1000	71	24
2000	35	3
5000	6	9
7000	0	0
10000	21	22

Table 12. IC_{50} values of TMZ in GBM cell lines A-172, U-251 MG, and LN-18 after 72 h of treatment.

Cell line	IC_{50}
	TMZ (µM)
A-172	5100

U-251 MG	2945
LN-18	1344

The results show higher IC_{50} values of TMZ in cell lines A-172 and U-251 MG compared to LN-18.

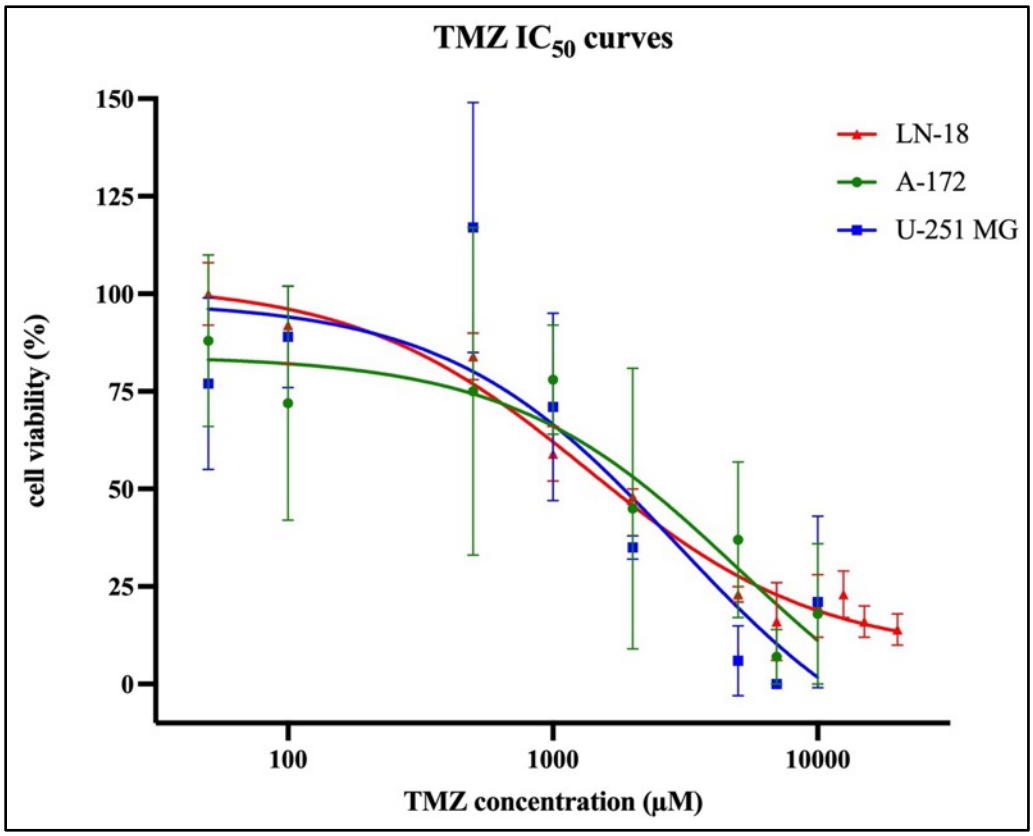

Figure 6. TMZ IC_{50} curves of GBM cell lines A-172 (green), U-251 MG (blue), and LN-18 (red) after 72 h of treatment with increasing TMZ concentrations. All data points are shown as a mean from n = 3 ± SD in LN-18 and U-251 MG and n = 6 ± SD in A-172.

4.2 IC_{50} curves of Gem

In each experimental run, 4,000 cells per well were seeded in cell lines A-172 and LN-18, and 1,500 cells per well were seeded for cell line U-251 MG, using 200 µL medium per well. Three wells were used for each concentration. The treatment lasted for 72 h and the cell viability after treatment was assessed using the MTS assay. All data was corrected against a blank well containing only medium and MTS assay reagents to account for and to substract the optical density of the reagents from the final readings obtained for the samples. To depict the Gem IC_{50} curves of all cell lines as accurately as possible, the mean values of cell viability

from both experimental runs of each cell line were calculated and are graphically presented in Figure 7.

Table 13. Mean cell viability (%) and SD in GBM cell line LN-18 after 72 h treatment with increasing Gem concentration and n = 3 from one experimental run.

Gem concentration (µM)	Mean cell viability (%)	SD (%)
0	100	1
0.0001	110	5
0.001	115	6
0.01	114	4
0.1	82	0
1	87	4
5	91	6
10	57	4
50	46	0
100	47	2
1000	20	1

Table 14. Mean cell viability (%) in GBM cell line A-172 after 72 h of treatment with different Gem concentrations. The data is shown as mean of n = 6 ± SD from two independent experimental runs.

Gem concentration (µM)	Mean cell viability (%)	SD (%)
0	111	11
0.0001	109	2
0.001	113	7
0.01	106	33
0.1	64	22
1	59	19
5	55	2
10	70	29
50	63	0
100	34	0

Table 15. Mean cell viability (%) and SD of GBM cell line U-251 MG after 72 h of treatment with different Gem concentrations. The mean cell viability was determined from n = 6 ± SD from two independent experimental runs.

Gem concentration (µM)	Mean cell viability (%)	SD (%)
0	100	0
0.0001	104	8
0.001	111	13
0.01	71	8
0.1	32	6
1	25	6
5	20	9
10	17	0
50	13	6
100	9	10

In all three GBM cell lines, there was a decrease in cell viability with increasing Gem concentration.

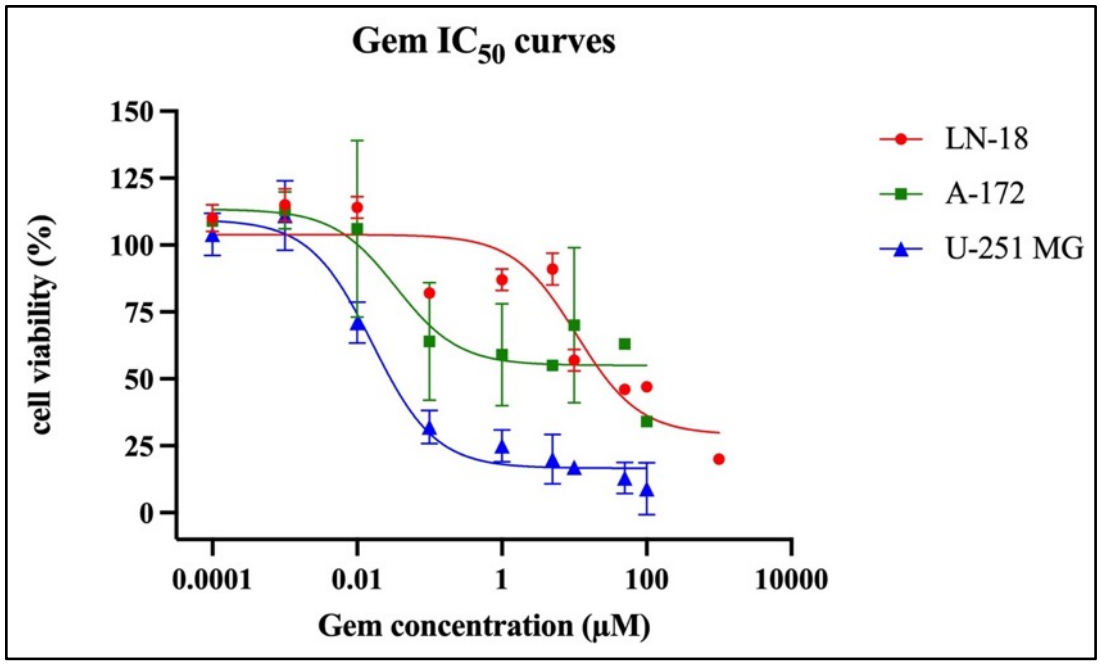

Figure 7. Comparison of all Gem-IC_{50} curves of GBM cell lines A-172 (green), U-251 MG (blue), and LN-18 (red) after 72 h of treatment. All data points for A-172 and U-251 are shown

as a mean of n = 6 from two experimental runs, while all data points for LN-18 are shown as a mean of n = 3 ± SD from one experimental run.

Table 16. IC_{50} values of Gem in GBM cell lines A-172, U-251 MG, and LN-18

Cell line	IC_{50}
	Gem (µM)
A-172	0.0344
U-251 MG	0.0163
LN-18	10.75

The IC_{50} values for Gem in the selected GBM cell lines lie in a sub-µM range, except for cell line LN-18. In comparison to the IC_{50} values of TMZ in the same cell lines, the Gem IC_{50} values were up to 10^{-5}-fold lower.

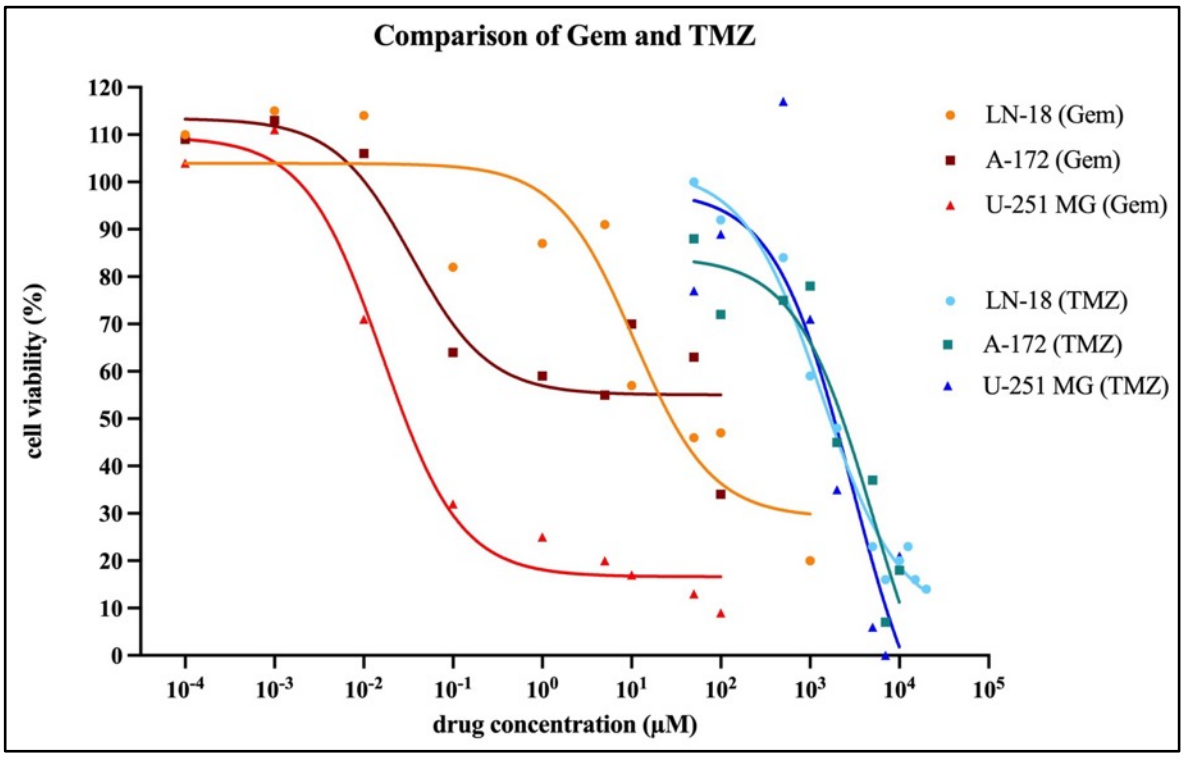

Figure 8. IC_{50} curves of Gem and TMZ in all three GBM cell lines in comparison, data re-used from figure 6 and figure 7. All cells were treated for 72 hours, and cell viability was assessed using the MTS assay. The labeling of SD was omitted to ensure better clarity and overview.

4.3 CAM assay results

For the CAM assay, the GBM cell line LN-18 was used. Each onplant consisted of 15 µL cell suspension containing 10^6 cells and 5 µL Matrigel® in CAM assays #169 or 5 µL Geltrex™ in CAM assays #174 and #175. As outlined in Chapter 3.4.4, the cells were seeded on the CAM before the eggs were incubated for 24 h to facilitate tumor cell adhesion and tumor formation. After 24 h, the LN-18 xenografts were treated with a single dose of 100 µM Gem or 1.5 mM TMZ and were further incubated for 72 h. The GC did not receive treatment. Subsequently, the xenografts were harvested, paraffin-embedded, and sliced to produce microscopic slides for further analysis.

4.3.1 HE staining

To derive an approximate microscopic overview of tumor growth on CAM and to examine tumor morphology, routine HE staining was performed. Figure 9 exemplifies the key components of a xenografted LN-18 tumor in the untreated GC group in which the black arrow points to the GBM onplant and the green arrows highlight the CAM. Furthermore, the red arrows show blood vessels, which provide a continuous blood supply to the tumor.

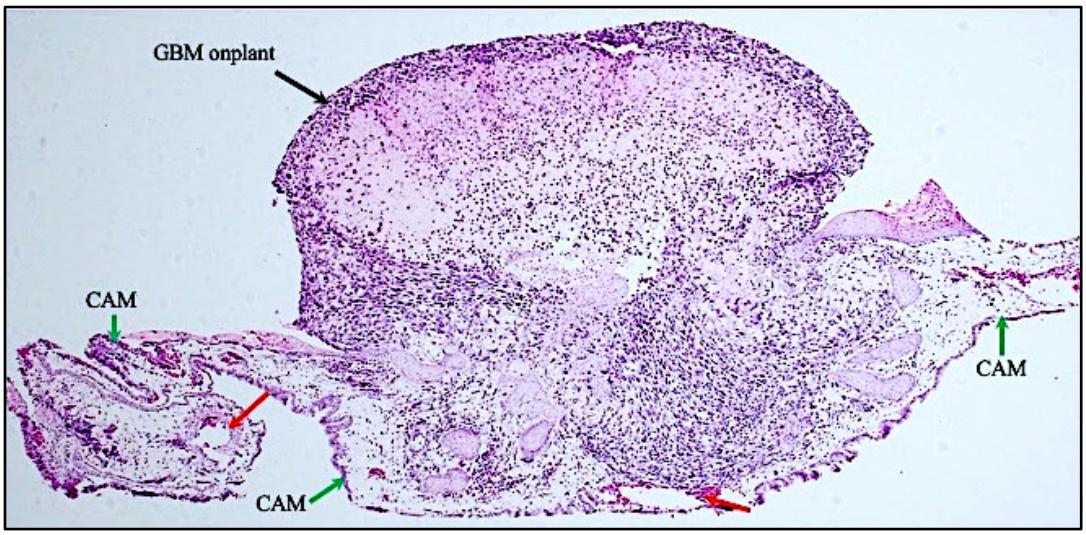

Figure 9. Untreated tumor of the cell line LN-18 on CAM as a representative of the xenografts (4x magnification). The arrows highlight the key components CAM (green arrows), blood vessels (red arrows), and the tumor itself (black arrow).

The HE-stained slides facilitated the selection of suitable slides for further immunohistochemical staining, whereby it should be noted that color variations are

attributed to the light source of the microscope and differences in the camera settings used during slide photography and have no impact on the data.

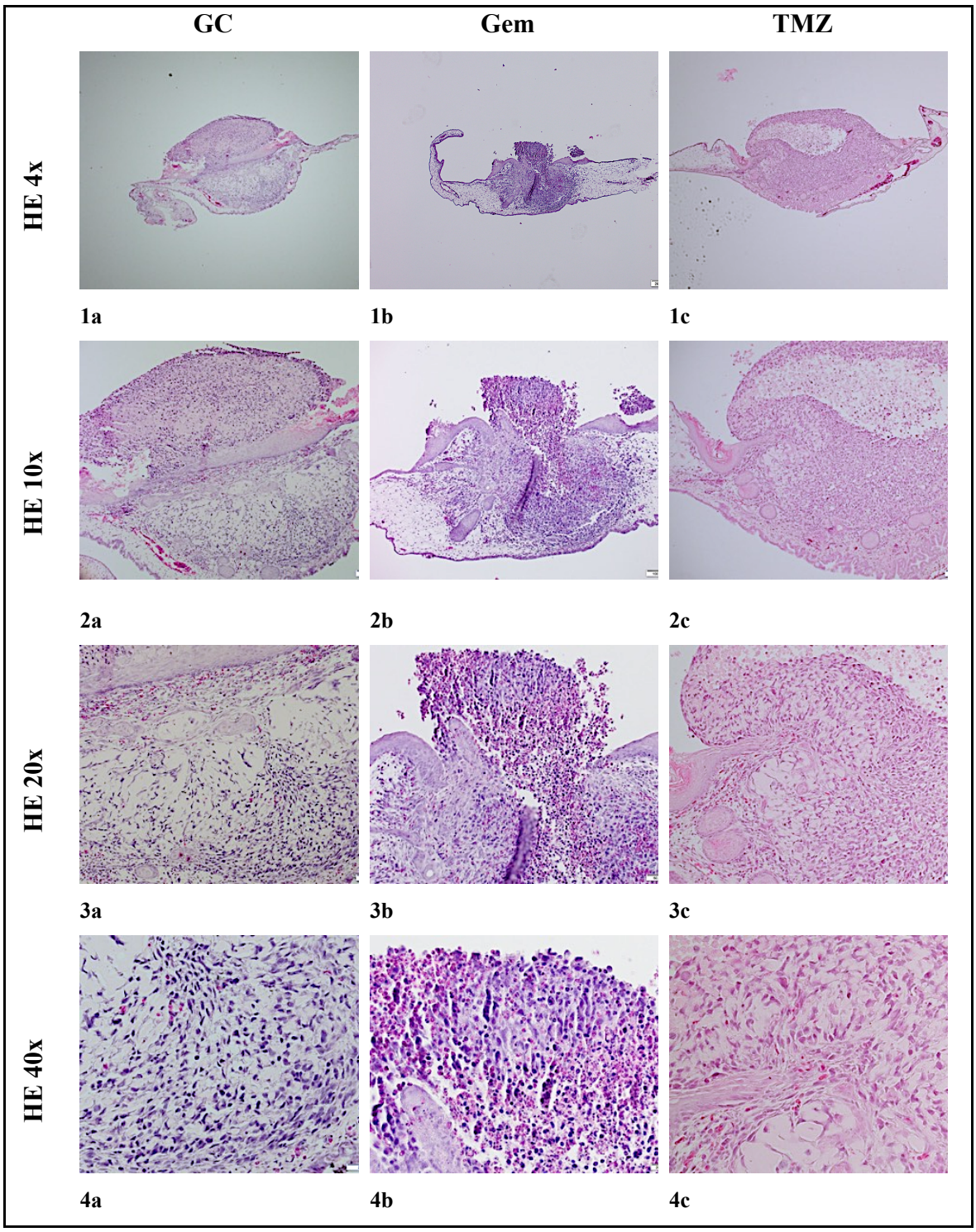

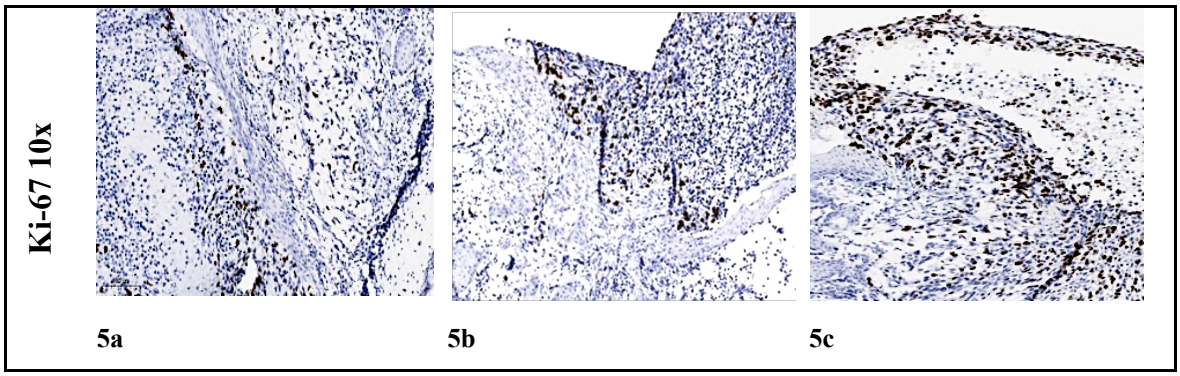

Figure 10. Images 1-4 are representative results of the HE-stained LN-18 xenografts from all three treatment conditions. Images 5a-c show each tumor in their respective Ki-67 staining. Each tumor is photographed in 4x, 10x, 20x and 40x magnification and their respective Ki-67 stain. Images 1-5a shows a xenograft of the GC group, Images 1-5b shows a tumor treated with Gem 100 µM and Images 1-5c shows the tumor treated with 1.5 mM TMZ. Images 3a-c show the invasion of tumor cells into the CAM.

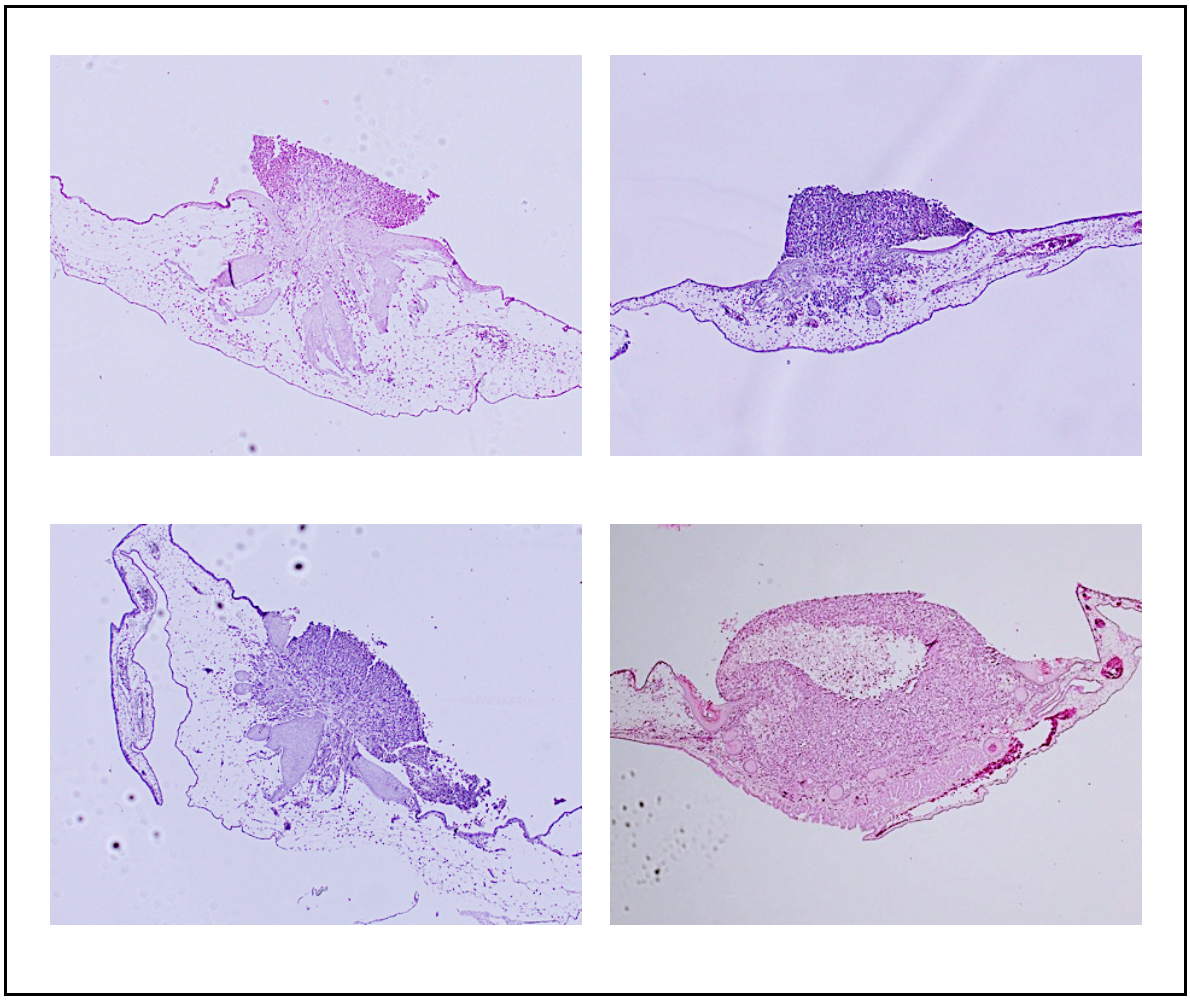

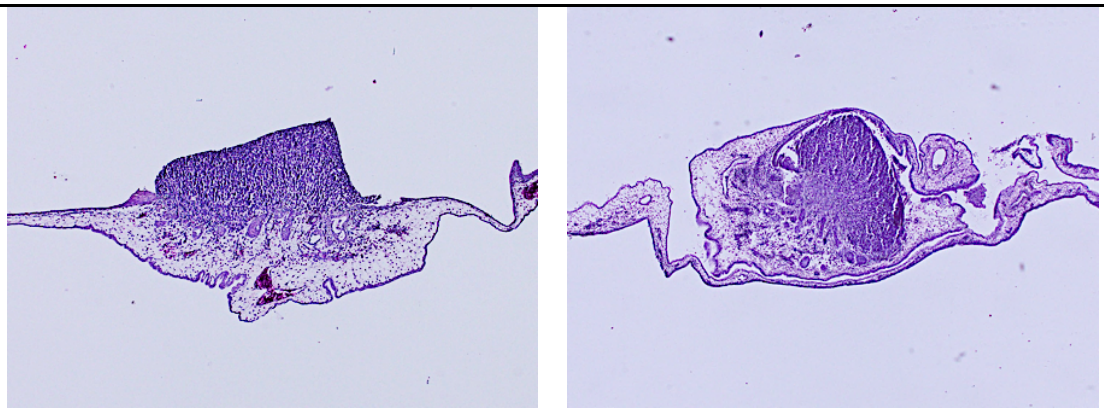

Figure 11. HE-stained LN-18 tumors on CAM treated with a single topical treatment of 20 µL solution with a TMZ concentration of 1.5 mM, followed by 72 h of incubation, displayed in 4x magnification.

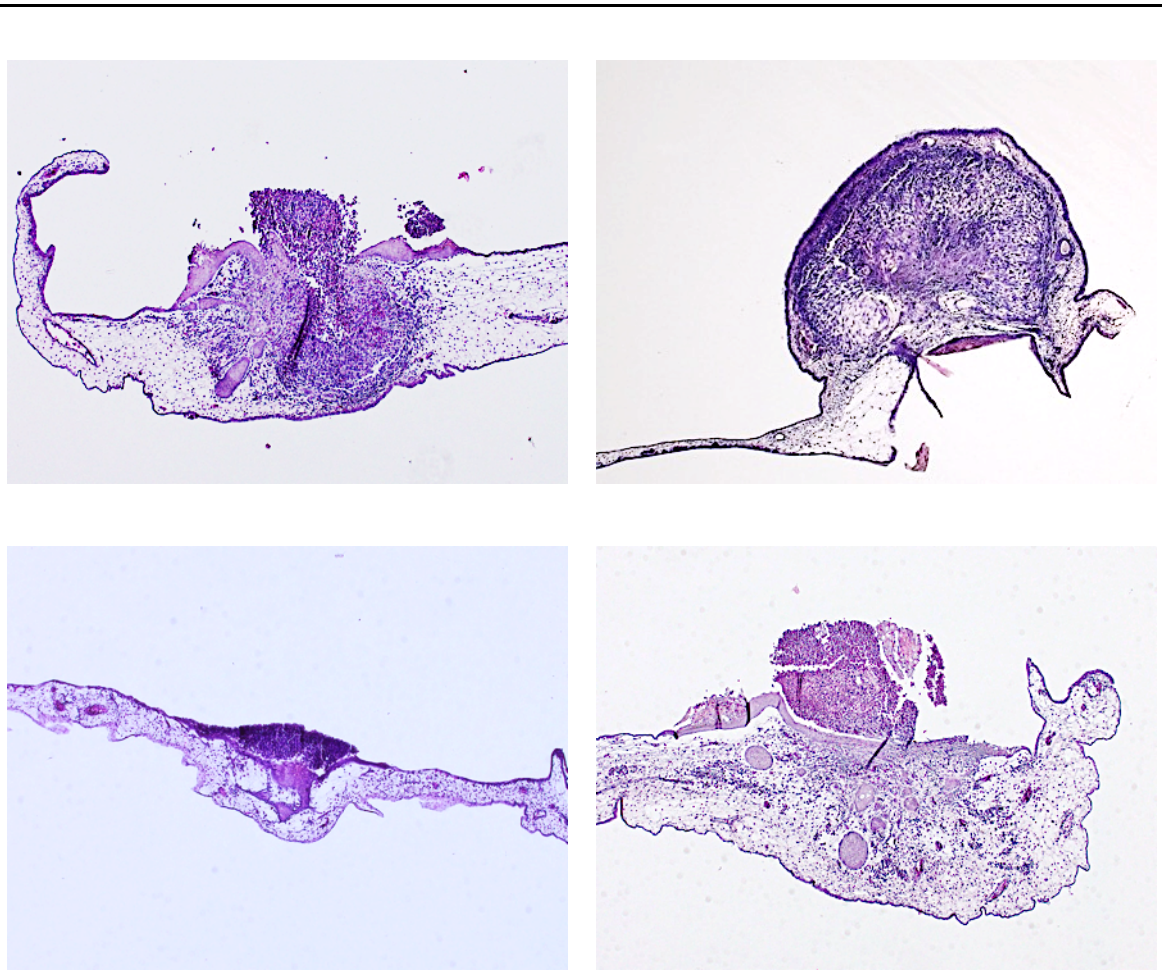

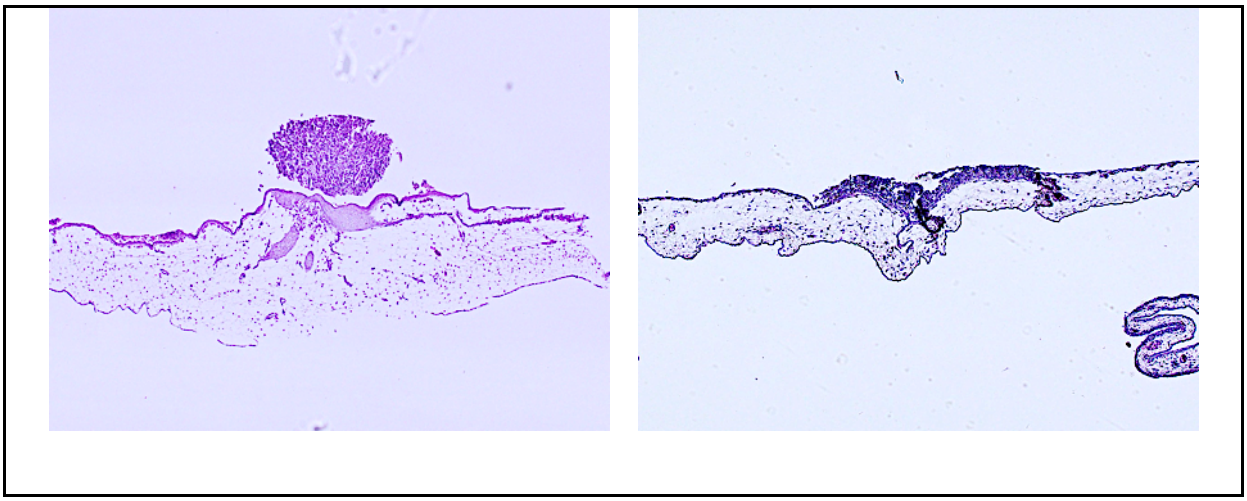

Figure 12. HE-stained slides with tumors of GBM cell line LN-18 on CAM after one single topical treatment with 20 µL of Gem in 100 µM concentration, followed by 72 h of incubation (4x magnification). Gem-treated tumors were prone to breakage while slicing and the superficial tumor on the CAM showed breakage and less density compared to those in the GC group. An invasion of the GBM cells in the CAM was observed.

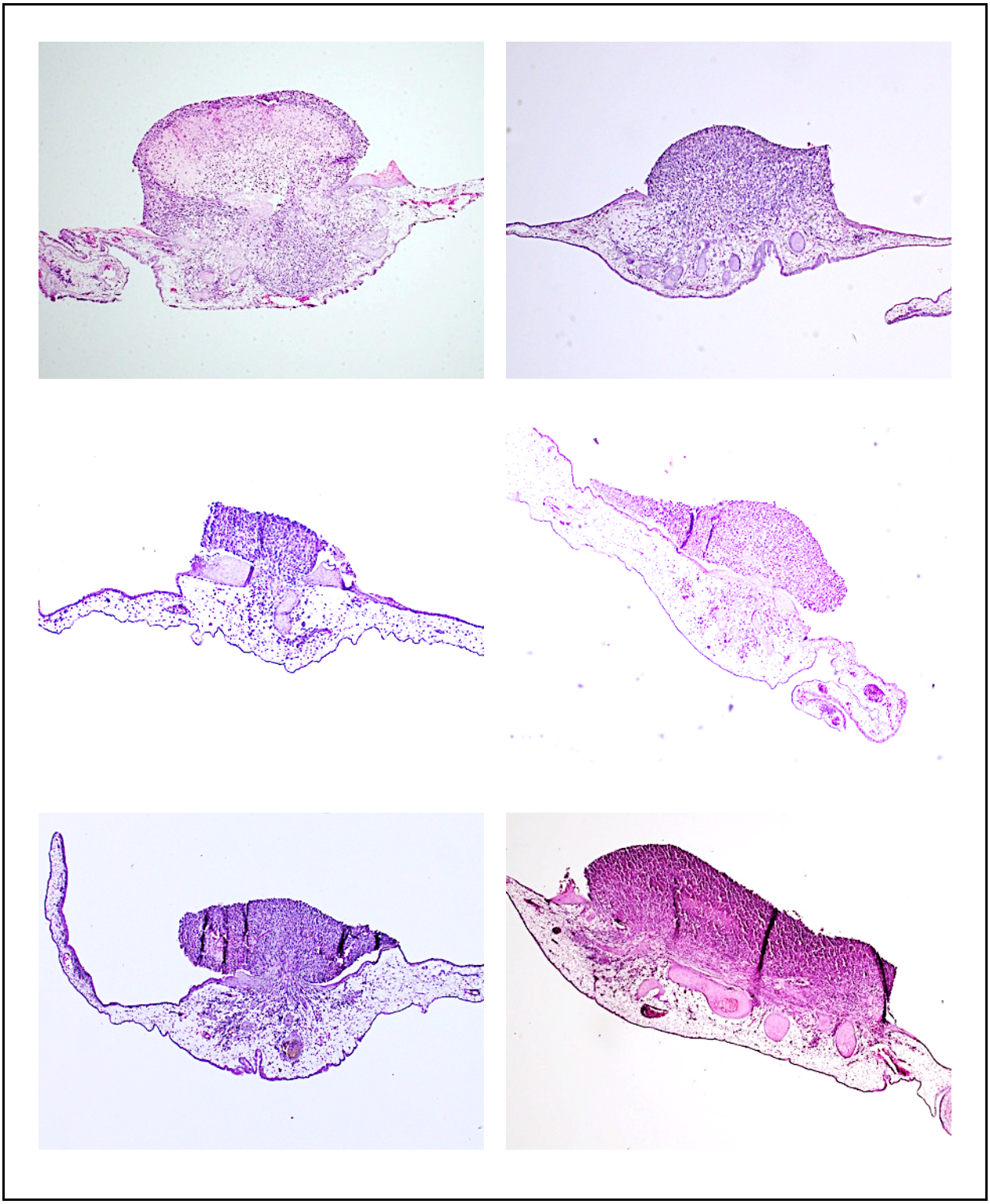

Figure 13. LN-18 tumors on CAM in the GC group received no treatment with any drug and were incubated for 72 h alongside the two treatment groups (HE-staining, 4x magnification). The untreated xenografts have a dense tissue composition and show a pronounced tumor cell invasion into the CAM.

The images presented in Figures 11, 12, and 13 indicate that a microscopic difference between the treatment groups was observable in the HE-stained slides. In comparison to the

TMZ treatment group, the Gem treatment group exhibited a distinct tendency to disintegrate whilst sectioning the paraffin-embedded xenografts, that was however not observed in analogous experiments with onplanted U-87 MG cells (unpublished results).

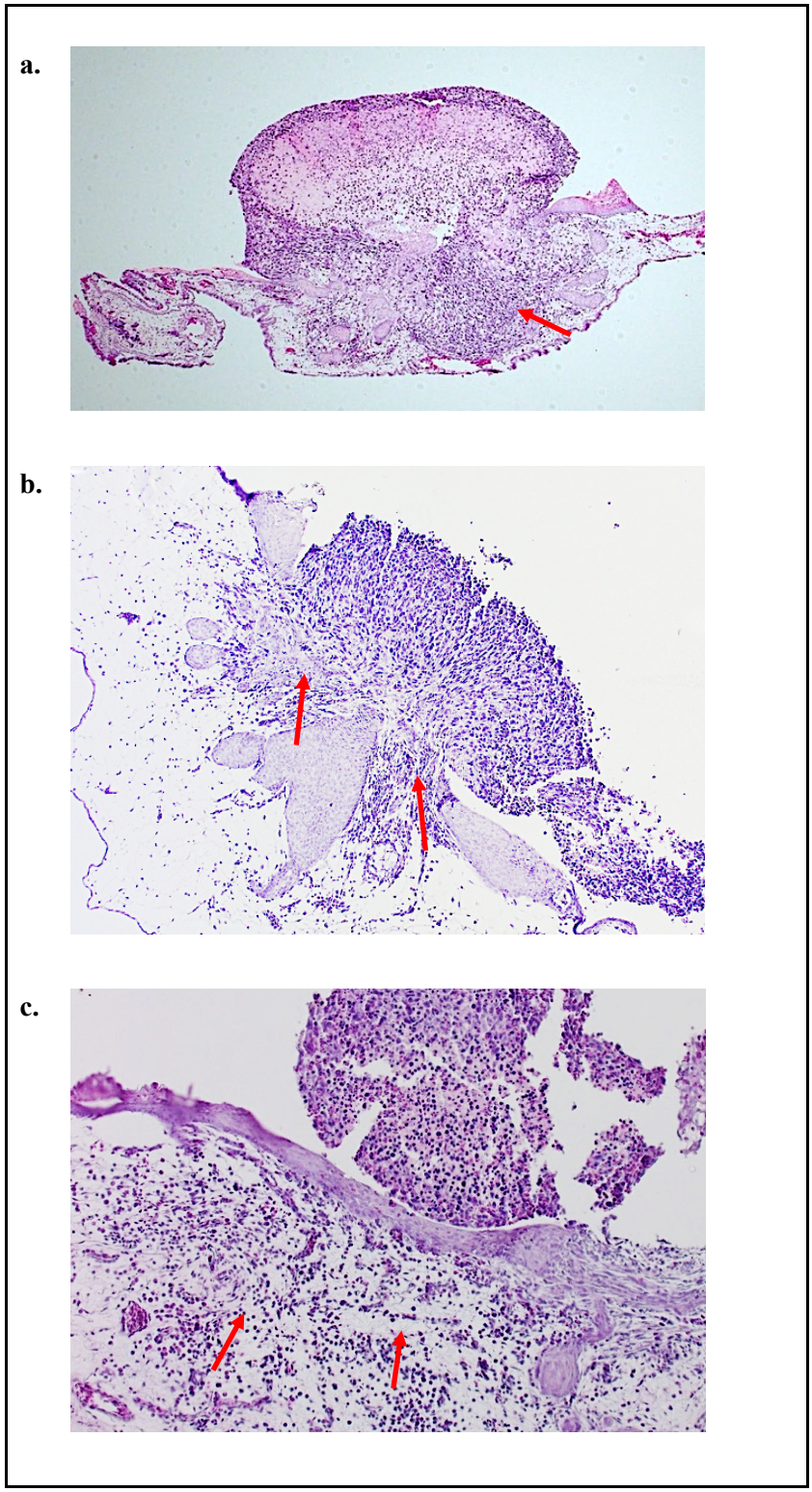

Figure 14. Microscopic comparison of an HE-stained slide of one xenograft of the untreated GC group in Image a (4x magnification) and one xenograft in the Gem group in Image b (10x magnification). Gem-treated tumors were more prone to breakage on the surface as shown in

Figures 14c and 15. All three treatment groups showed tumor invasion into the CAM (red arrows).

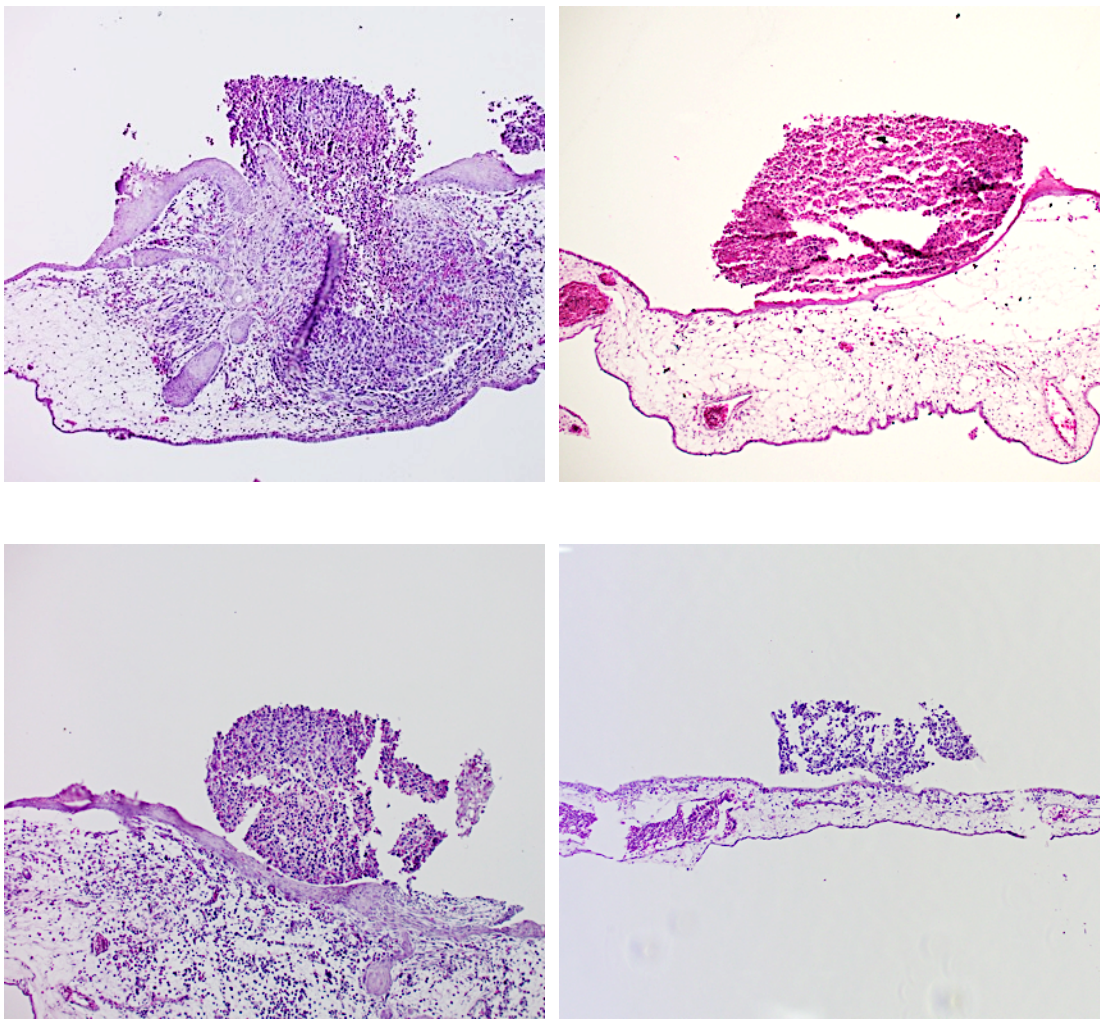

Figure 15. HE-slides of Gem-treated LN-18 tumors on CAM with low tumor cell cohesion in x10 magnification. The Gem-treated tumors exhibited a higher susceptibility to breakage, both during tumor harvesting and the subsequent slicing process for preparing microscopic slides.

4.3.2 Ki-67 proliferation index

The Ki-67 proliferation index is a well-established immunohistochemical marker for cell proliferation and is used as both a prognostic and predictive tumor marker in cancer research (47). The Ki-67 protein serves as a cellular marker for cell proliferation, as it is associated with ribosomal ribonucleic acid (RNA) synthesis (48). It is expressed during the G1, S, G2, and M phases of the cell cycle, but not during the G0 phase (48). Ki-67 reaches its highest levels in mitosis, when the cell's nucleoplasm dissipates, and the protein relocates to the chromosomal surface (49). At this stage, it can be marked with an antibody and subsequently detected, whereby the percentage of positive Ki-67 detected is directly proportional to the number of proliferating cells (48).

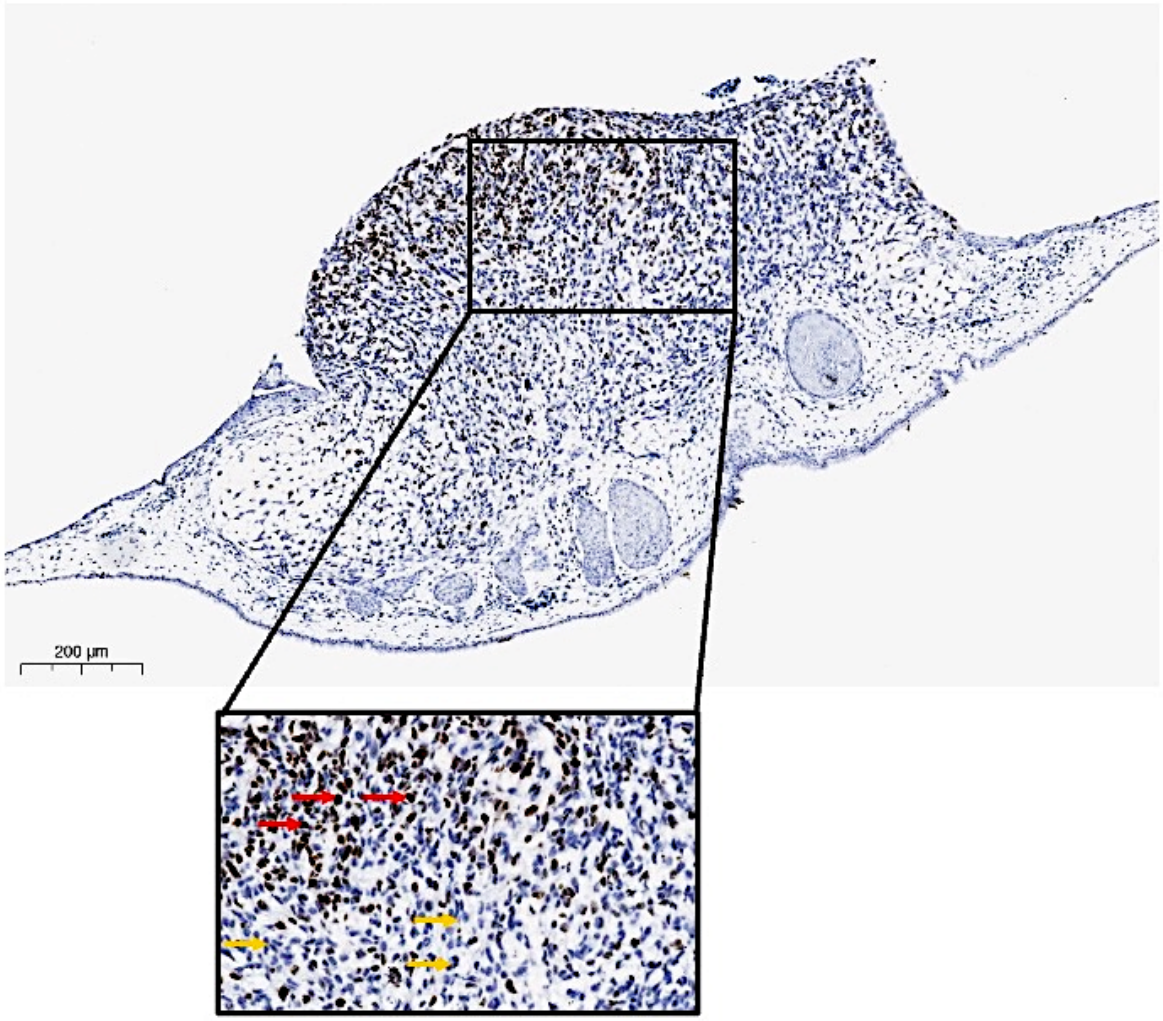

Figure 16. Ki-67 stained GBM tumor of cell line LN-18 on CAM for reference (10x magnification). In the zoomed area (16.4x magnification) Ki-67 positive cells are brown (red arrows) while Ki-67 negative cells are blue (yellow arrows).

4.3.3 Immunohistochemical quantification – statistical evaluation of the Ki-67 proliferation index

To perform the statistical evaluation of the collected data, the Shapiro-Wilk test was used to assess their normal distribution. The number of samples includes 14 samples from the GC group, 12 of samples treated with 100 µM Gem, and 15 samples treated with 1.5 mM TMZ.

Table 17. The Shapiro-Wilk test of gathered data does not indicate a normal distribution.

	Ki-67 proliferation index (%)		
	GC	Gem	TMZ
N	14	12	15
Shapiro-Wilk	0.886	0.844	0.853
P-value of Shapiro-Wilk	0.072	0.031	0.019

The Shapiro-Wilk test does not indicate a normal distribution within the treatment groups Gem and TMZ, as a normal distribution is defined as a Shapiro-Wilk p-value (p) > 0.05. As two outliers in the respective treatment group Gem and TMZ were observable, an outlier analysis was additionally performed, and two data points removed from the data set. Subsequently, the Shapiro-Wilk test was repeated and showed a normal distribution in the data after outlier correction, with a GC p = 0.072, a Gem p = 0.537 and a TMZ p = 0.134.

Table 18. The Shapiro-Wilk test showed normal distribution after outlier correction.

	Ki-67 proliferation index (%)		
	GC	Gem	TMZ
N	14	11	14
Shapiro-Wilk	0.886	0.941	0.905
P-value of Shapiro-Wilk	0.072	0.537	0.134

Table 19. The median and mean Ki-67 indexes (%) of LN-18 tumors that were determined for three treatment conditions: Gem 100 µM, TMZ 1.5 mM, and a GC group with no treatment. The results were obtained by using the QuPath software to accurately identify the Ki-67 positive cells following immunohistochemical staining.

	Ki-67 proliferation index (%)		
	GC	Gem	TMZ
N	14	11	14
Median	6.64	4.40	4.54
Mean	8.19	4.81	5.99
SD	6.28	3.77	4.42

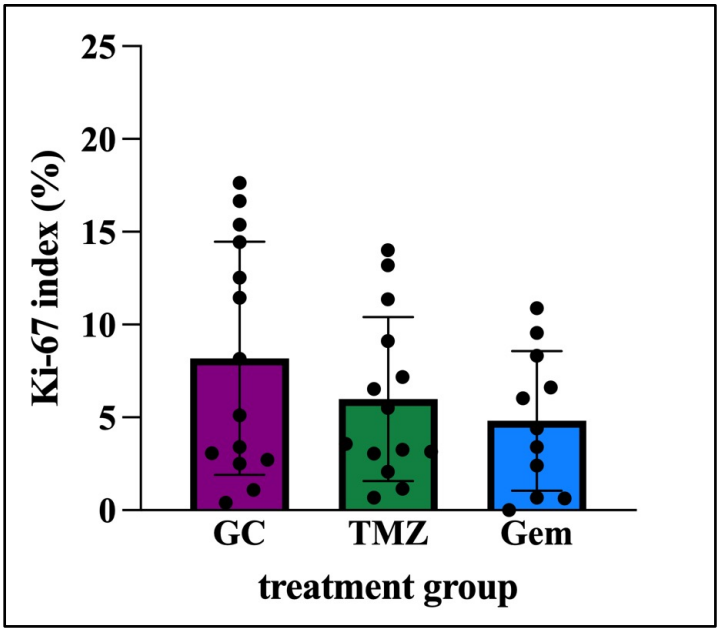

Figure 17. Box plot of the Ki-67 indexes of all treatment groups with the SD and distribution of individual Ki-67 index values within each treatment group.

Levene's test yielded a significant $p = 0.022$, suggesting heterogeneity of variances among the treatment groups. While a normal distribution was present within the data, the Kruskal-Wallis test was employed to calculate the p due to the unequal variances observed in the collected data, as indicated by Levene's test. The statistical significance of the differences between the three treatment groups was established at a p-threshold of $p < 0.05$, and the degrees of freedom (df) are 2. The H-value (H) is 1.75 which indicates no significant difference between the treatment groups. The Kruskal-Wallis test yielded a $p = 0.417$, which is not considered significant. The statistical results are presented in Table 19 and Table 20.

Table 20. The results derived from the Kruskal-Wallis test to determine the p of the CAM assays of the three treatment groups (Gem, TMZ, and GC group).

Factor	H	df	p
Treatment group	1.75	2	0.417

5 Discussion

The utilization of the OEIP for a local chemotherapeutic approach offers the capability to administer precise, localized, and targeted drug treatments. This approach ensures accurate and focused drug delivery without the need for solvent solutions, thus minimizing the adverse effects on brain tissue and spatial interference (31–33). Given the capability of the OEIP to directly deliver chemotherapeutic agents to the target site in the brain, the BBB that limits chemotherapeutic drug options could be circumvented, potentially expanding the availability of novel treatment agents.

This treatment concept could have the potential to enhance patients' quality of life and potentially extend their overall survival. Although Gem previously demonstrated an anticlonogenic and cytotoxic effect on GBM cells, its widespread clinical application is impeded by its limited ability to cross the BBB (40). Due to its potential in novel GBM treatment approaches, Gem was selected for closer examination because of its putative compatibility with an OEIP application.

The objective of this study was thus to evaluate the suitability of Gem as a chemotherapeutic for potential future OEIP application in three GBM cell lines and compare its efficacy to the established gold standard TMZ.

The results show that Gem had up to 10^{-5} times lower IC_{50} values compared to TMZ in *in vitro* experiments conducted on GBM cell lines A-172, U-251 MG, and LN-18. According to the findings derived from the *in vitro* experiments, Gem exhibited a pronounced anti-tumor effect by reducing the tumor cell proliferation and mean cell viability of GBM cell lines at considerably lower concentrations compared to TMZ. These outcomes are consistent with studies conducted by Genç et al. (50) on the Gli-6 GBM cell line and Waldherr et al. (33) on the U-251 and U-87 GBM cell lines. The IC_{50} values of Gem for U-87 and U-251 MG were found to be 0.01 µM and 0.02 µM (33), respectively, which closely align with the results of this study, in which U-251 MG exhibited an IC_{50} value of Gem of 0.0163 µM. Gem's IC_{50} values of the GBM cell line Gli-6 was assessed under both monolayer and spheroid conditions with a 24 h incubation period and resulted in IC_{50} values of 0.03 µM (50).

The consistent IC_{50} values in different studies and across different GBM cell lines indicate the potential effectiveness of Gem as an anti-neoplastic agent, particularly given its lower concentration requirements compared to TMZ.

To evaluate this effect under *in vivo* conditions, a 3D tumor model using the CAM-assay was implemented that utilized LN-18 cell line-derived tumors. Within this model, cell line LN-18 developed round, solid tumors on the CAM, accompanied by invasive behavior. These tumors were subjected to a single topical treatment of either 100 µM Gem or 1.5 mM TMZ, while an untreated GC group was also included. In the microscopical analysis of the HE-stained tumor slides, a noticeable difference was observed between Gem-treated and TMZ-treated tumors as Gem-treated tumors displayed an increased susceptibility to breakage during the harvesting and the preparation of the xenografts for microscopic slides (see Figure 14). To assess the impact of Gem and TMZ on the proliferation capacity of GBM cells (LN-18), immunohistochemical staining was performed and the Ki-67 proliferation index was determined by using the QuPath bioimage analysis software (45). From the statistical analysis, no statistically significant disparity between the effects of Gem, TMZ, and the no treatment condition (control) was observed ($p = 0.417$). This outcome underscores that a single once-off treatment of GBM LN-18 cells is not sufficient to yield significant outcomes.

However, to establish and quantify a confirmed correlation between Gem treatment and reduced tumor cell cohesion in LN-18 GBM tumors, additional investigations and subsequent statistical analyses are required. Given that this observation did not correspond to a reduced Ki-67 proliferation index in the GBM tumors, we refrained from pursuing further correlations.

Despite the established anti-neoplastic effects of Gem and TMZ, a one-time treatment seems inadequate to effectively inhibit tumor growth. Since neither Gem nor TMZ led to a statistically significant reduction in proliferation rate within the CAM-assay, considering a modification of the treatment regimen may thus be warranted. As demonstrated in a recent study by Rupp et al. (42), multiple treatments of a GBM xenograft on CAM with TMZ resulted in a significant reduction in the tumor's weight (42).

In the study by Waldherr et al. (33), IC_{50} values for Gem and TMZ were determined for astrocytes and neurons and the respective examined cells exhibited a significantly lower sensitivity to Gem compared to TMZ (33). Due to the wide therapeutic range of Gem,

modification of the treatment concept in terms of repetitive drug administration or dose escalation would therefore be feasible.

Expanding the treatment regimen of the CAM assay employed in this work to include repeated treatments or treatments with increased concentrations of the chemotherapeutic agents could possibly provide further insights into the comparative efficacy of Gem and TMZ on GBM cells. Another potential approach to expand the anti-neoplastic treatment could be to incorporate a radiotherapeutic regimen, capitalizing on Gem's potential as a potent radiosensitizer.

In conclusion, the iontronic drug delivery facilitated by the OEIP demonstrates a reliable capability for precise administration (31–33). In an attempt to develop iontronic devices for GBM treatment, this *in vitro* study demonstrated Gem's superior antineoplastic potency against three GBM cell lines, surpassing TMZ. While the Ki-67 index outcomes among treatment groups in the CAM assay remained inconclusive, studies indicate the possibility of a more promising outcome through the modification of the treatment regimen. However, the advancement of OEIPs for clinical application remains a work in progress. Furthermore, the exploration of alternative chemotherapeutic agents compatible with the device holds potential and might surpass Gem's suitability for treatment.

As GBM is regarded as an affliction of the entire brain due to its well-characterized invasiveness, localized treatment options could be just one facet of a multifaceted approach toward successfully treating this disease (51). While further development and optimizations are required, iontronic devices hold great promise as a novel and potentially advantageous concept in clinical cancer treatment.

References

(1) Höfler G, Kreipe HH, Moch H. Pathologie: das Lehrbuch : mit 1.300 meist farbigen Abbildungen und rund 150 Tabellen. 2019.

(2) Vleeschouwer S de. Glioblastoma [Internet]. 2017 [cited 2020 Jun 5]. Available from: http://www.ncbi.nlm.nih.gov/books/NBK469998/

(3) Louis DN, Perry A, Reifenberger G, von Deimling A, Figarella-Branger D, Cavenee WK, et al. The 2016 World Health Organization Classification of Tumors of the Central Nervous System: a summary. Acta Neuropathol (Berl). 2016 Jun;131(6):803–20.

(4) Louis DN, Perry A, Wesseling P, Brat DJ, Cree IA, Figarella-Branger D, et al. The 2021 WHO Classification of Tumors of the Central Nervous System: a summary. Neuro-Oncol. 2021 Aug 2;23(8):1231–51.

(5) Organisation mondiale de la santé, Centre international de recherche sur le cancer, editors. Central nervous system tumours. 5th ed. Lyon: International agency for research on cancer; 2021. (World health organization classification of tumours).

(6) Greenberg MS. Handbook of neurosurgery. 2020.

(7) Morris M, Rodriguez FJ. Glioblastoma, IDH mutant. PathologyOutlines.com [Internet]. 2020. Available from: http://www.pathologyoutlines.com/topic/cnstumorglioblastomaidhmutant.html

(8) Thakkar JP, Dolecek TA, Horbinski C, Ostrom QT, Lightner DD, Barnholtz-Sloan JS, et al. Epidemiologic and Molecular Prognostic Review of Glioblastoma. Cancer Epidemiol Biomarkers Prev. 2014 Oct 1;23(10):1985–96.

(9) Sloane D. Cancer Epidemiology in the United States: Racial, Social, and Economic Factors. In: Verma M, editor. Cancer Epidemiology [Internet]. Totowa, NJ: Humana Press; 2009 [cited 2020 Jun 5]. p. 65–83. (Walker JM, editor. Methods in Molecular Biology; vol. 471). Available from: http://link.springer.com/10.1007/978-1-59745-416-2_4

(10) Wrensch M, Minn Y, Chew T, Bondy M, Berger MS. Epidemiology of primary brain tumors: current concepts and review of the literature. Neuro-Oncol. 2002;4(4):278–99.

(11) Furnari FB, Fenton T, Bachoo RM, Mukasa A, Stommel JM, Stegh A, et al. Malignant astrocytic glioma: genetics, biology, and paths to treatment. Genes Dev. 2007 Nov 1;21(21):2683–710.

(12) Santarpia L, Lippman SM, El-Naggar AK. Targeting the MAPK–RAS–RAF signaling pathway in cancer therapy. Expert Opin Ther Targets. 2012 Jan;16(1):103–19.

(13) Li X, Wu C, Chen N, Gu H, Yen A, Cao L, et al. PI3K/Akt/mTOR signaling pathway and targeted therapy for glioblastoma. Oncotarget. 2016 May 31;7(22):33440–50.

(14) Harris SL, Levine AJ. The p53 pathway: positive and negative feedback loops. Oncogene. 2005 Apr;24(17):2899–908.

(15) Hegi ME, Diserens AC, Gorlia T, Hamou MF, de Tribolet N, Weller M, et al. MGMT Gene Silencing and Benefit from Temozolomide in Glioblastoma. N Engl J Med. 2005 Mar 10;352(10):997–1003.

(16) Strobel H, Baisch T, Fitzel R, Schilberg K, Siegelin MD, Karpel-Massler G, et al. Temozolomide and Other Alkylating Agents in Glioblastoma Therapy. Biomedicines. 2019 Sep 9;7(3):69.

(17) Hegi ME, Liu L, Herman JG, Stupp R, Wick W, Weller M, et al. Correlation of O ^{6} -Methylguanine Methyltransferase (MGMT) Promoter Methylation With Clinical Outcomes in Glioblastoma and Clinical Strategies to Modulate MGMT Activity. J Clin Oncol. 2008 Sep 1;26(25):4189–99.

(18) Lee SY. Temozolomide resistance in glioblastoma multiforme. Genes Dis. 2016 Sep;3(3):198–210.

(19) Advances in biology and treatment of glioblastoma. New York, NY: Springer Science+Business Media; 2017.

(20) Department of Neurosurgery, Jordan University Hospital and Medical School, University of Jordan, Amman, Jordan, Tamimi AF, Juweid M, Department of Radiology and Nuclear Medicine, Jordan University Hospital and Medical School, University of Jordan, Amman, Jordan. Epidemiology and Outcome of Glioblastoma. In: Department of Neurosurgery, University Hospitals Leuven, Leuven, Belgium, De Vleeschouwer S, editors. Glioblastoma [Internet]. Codon Publications; 2017 [cited 2020 Jun 10]. p. 143–53. Available from: https://exonpublications.com/index.php/exon/article/view/130

(21) Hanif F, Muzaffar K, Perveen kahkashan, Malhi S, Simjee S. Glioblastoma Multiforme: A Review of its Epidemiology and Pathogenesis through Clinical Presentation and Treatment. Asian Pac J Cancer Prev [Internet]. 2017 Jan [cited 2021 Sep 13];18(1). Available from: https://doi.org/10.22034/APJCP.2017.18.1.3

(22) McKinnon C, Nandhabalan M, Murray SA, Plaha P. Glioblastoma: clinical

presentation, diagnosis, and management. BMJ. 2021 Jul 14;n1560.

(23) Alifieris C, Trafalis DT. Glioblastoma multiforme: Pathogenesis and treatment. Pharmacol Ther. 2015 Aug 1;152:63–82.

(24) Batash R, Asna N, Schaffer P, Francis N, Schaffer M. Glioblastoma Multiforme, Diagnosis and Treatment; Recent Literature Review. Curr Med Chem [Internet]. 2017 Sep 21 [cited 2020 Mar 31];24(27). Available from: http://www.eurekaselect.com/152454/article

(25) Wang JL, Mugge L, Giglio P, Puduvalli VK. Current Therapies and Future Directions in Treatment of Glioblastoma. In: Somasundaram K, editor. Advances in Biology and Treatment of Glioblastoma [Internet]. Cham: Springer International Publishing; 2017 [cited 2021 Oct 19]. p. 57–89. (Current Cancer Research). Available from: http://link.springer.com/10.1007/978-3-319-56820-1_3

(26) Adamson C, Kanu OO, Mehta AI, Di C, Lin N, Mattox AK, et al. Glioblastoma multiforme: a review of where we have been and where we are going. Expert Opin Investig Drugs. 2009 Aug;18(8):1061–83.

(27) Wick W. et al. Gliome, S2k-Leitlinie, 2021 [Internet]. Deutsche Gesellschaft für Neurologie (Hrsg.), Leitlinien für Diagnostik und Therapie in der Neurologie; [cited 2022 Dec 5]. Available from: www.dgn.org/leitlinien

(28) Bregy A, Shah AH, Diaz MV, Pierce HE, Ames PL, Diaz D, et al. The role of Gliadel wafers in the treatment of high-grade gliomas. Expert Rev Anticancer Ther. 2013 Dec;13(12):1453–61.

(29) Fabian D, Guillermo Prieto Eibl M, Alnahhas I, Sebastian N, Giglio P, Puduvalli V, et al. Treatment of Glioblastoma (GBM) with the Addition of Tumor-Treating Fields (TTF): A Review. Cancers. 2019 Feb 2;11(2):174.

(30) Seitanidou M, Franco-Gonzalez JF, Sjöström TA, Zozoulenko I, Berggren M, Simon DT. pH Dependence of γ-Aminobutyric Acid Iontronic Transport. J Phys Chem B. 2017 Aug 3;121(30):7284–9.

(31) Arbring Sjöström T, Berggren M, Gabrielsson EO, Janson P, Poxson DJ, Seitanidou M, et al. A Decade of Iontronic Delivery Devices. Adv Mater Technol. 2018 May;3(5):1700360.

(32) Seitanidou M, Tybrandt K, Berggren M, Simon DT. Overcoming transport limitations in miniaturized electrophoretic delivery devices. Lab Chip. 2019;19(8):1427–35.

(33) Waldherr L, Seitanidou M, Jakešová M, Handl V, Honeder S, Nowakowska M, et al.

Targeted Chemotherapy of Glioblastoma Spheroids with an Iontronic Pump. Adv Mater Technol. 2021 May;6(5):2001302.

(34) Jonsson A, Song Z, Nilsson D, Meyerson BA, Simon DT, Linderoth B, et al. Therapy using implanted organic bioelectronics. Sci Adv. 2015 May;1(4):e1500039.

(35) Poxson DJ, Karady M, Gabrielsson R, Alkattan AY, Gustavsson A, Doyle SM, et al. Regulating plant physiology with organic electronics. Proc Natl Acad Sci. 2017 May 2;114(18):4597–602.

(36) Seitanidou M, Blomgran R, Pushpamithran G, Berggren M, Simon DT. Modulating Inflammation in Monocytes Using Capillary Fiber Organic Electronic Ion Pumps. Adv Healthc Mater. 2019 Oct;8(19):1900813.

(37) Singh N, Miner A, Hennis L, Mittal S. Mechanisms of temozolomide resistance in glioblastoma - a comprehensive review. Cancer Drug Resist [Internet]. 2020 [cited 2023 Jan 23]; Available from: https://cdrjournal.com/article/view/3779

(38) Piper K, DePledge L, Karsy M, Cobbs C. Glioma Stem Cells as Immunotherapeutic Targets: Advancements and Challenges. Front Oncol. 2021 Feb 24;11:615704.

(39) Bastiancich C, Bastiat G, Lagarce F. Gemcitabine and glioblastoma: challenges and current perspectives. Drug Discov Today. 2018 Feb;23(2):416–23.

(40) Rieger J, Durka S, Streffer J, Dichgans J, Weller M. Gemcitabine cytotoxicity of human malignant glioma cells: modulation by antioxidants, BCL-2 and dexamethasone. Eur J Pharmacol. 1999 Jan;365(2–3):301–8.

(41) Ghaffari-Tabrizi-Wizsy N, Passegger CA, Nebel L, Krismer F, Herzer-Schneidhofer G, Schwach G, et al. The avian chorioallantoic membrane as an alternative tool to study medullary thyroid cancer. Endocr Connect. 2019 May;8(5):462–7.

(42) Rupp T, Legrand C, Hunault M, Genest L, Babin D, Froget G, et al. A Face-To-Face Comparison of Tumor Chicken Chorioallantoic Membrane (TCAM) In Ovo with Murine Models for Early Evaluation of Cancer Therapy and Early Drug Toxicity. Cancers. 2022 Jul 21;14(14):3548.

(43) Nowak-Sliwinska P, Segura T, Iruela-Arispe ML. The chicken chorioallantoic membrane model in biology, medicine and bioengineering. Angiogenesis. 2014 Oct;17(4):779–804.

(44) Kain KH, Miller JWI, Jones-Paris CR, Thomason RT, Lewis JD, Bader DM, et al. The chick embryo as an expanding experimental model for cancer and cardiovascular research: The Chick as an Experimental Model. Dev Dyn. 2014 Feb;243(2):216–28.

(45) Bankhead P, Loughrey MB, Fernández JA, Dombrowski Y, McArt DG, Dunne PD,

et al. QuPath: Open source software for digital pathology image analysis. Sci Rep. 2017 Dec 4;7(1):16878.

(46) JASP Team (2023). JASP (Version 0.17.3)[Computer software].

(47) Gerdes J, Schwab U, Lemke H, Stein H. Production of a mouse monoclonal antibody reactive with a human nuclear antigen associated with cell proliferation. Int J Cancer. 1983 Jan 15;31(1):13–20.

(48) Jonat W, Arnold N. Is the Ki-67 labelling index ready for clinical use? Ann Oncol. 2011 Mar;22(3):500–2.

(49) Wong E, Nahar N, Hau E, Varikatt W, Gebski V, Ng T, et al. Cut-point for Ki-67 proliferation index as a prognostic marker for glioblastoma. Asia Pac J Clin Oncol. 2019 Feb;15(1):5–9.

(50) Genç M, Castro Kreder N, Barten-van Rijbroek A, Stalpers LJA, Haveman J. Enhancement of effects of irradiation by gemcitabine in a glioblastoma cell line and cell line spheroids. J Cancer Res Clin Oncol. 2004 Jan 1;130(1):45–51.

(51) Agarwal S, Sane R, Oberoi R, Ohlfest JR, Elmquist WF. Delivery of molecularly targeted therapy to malignant glioma, a disease of the whole brain. Expert Rev Mol Med. 2011 May;13:e17.